Dalton Transactions

PAPER

View Article Online
View Journal | View Issue

Cite this: *Dalton Trans.*, 2017, **46**, 8992

Cr^{III} as an alternative to Ru^{II} in metallo-supramolecular chemistry†

Davood Zare,‡[a] Benjamin Doistau,*‡[a] Homayoun Nozary,[a] Céline Besnard,[b] Laure Guénée,[b] Yan Suffren,[c] Anne-Laure Pelé,[c] Andreas Hauser*[c] and Claude Piguet *[a]

Compared to divalent ruthenium coordination complexes, which are widely exploited as parts of multi-component photonic devices, optically active trivalent chromium complexes are under-represented in multi-metallic supramolecular architectures performing energy conversion mainly because of the tricky preparation of stable heteroleptic Cr^{III} building blocks. We herein propose some improvements with the synthesis of a novel family of kinetically inert heteroleptic bis-terdentate mononuclear complexes, which can be incorporated into dinuclear rod-like dyads as a proof-of-concept. The mechanism and magnitude of intermetallic Cr···Cr communication have been unraveled by a combination of magnetic, photophysical and thermodynamic investigations. Alternated aromatic/alkyne connectors provided by Sonogashira coupling reactions emerge as the most efficient wires for long-distance communication between two chromium centres bridged by Janus-type back-to-back bis-terdentate receptors.

Received 12th May 2017,
Accepted 8th June 2017

DOI: 10.1039/c7dt01747b

rsc.li/dalton

Introduction

Since the discovery of chromium by Louis Nicolas Vauquelin in 1798, chromium derivatives, particularly in their most stable oxidation state Cr^{III}, have been widely studied for their catalytic,[1–3] hole transfer ability in photo-cathodic solar cells,[4,5] magnetic,[6–12] and optical properties.[13–15] The latter aspect culminated with the building of the first laser in 1960,[16] which exploited the stimulated emission of electromagnetic radiation from the Cr^{III}-centred excited levels found in ruby. Despite its appealing electronic properties, Cr^{III} has been scarcely introduced into polymetallic supramolecular architectures working as photonic devices,[17,18] whereas hundreds, if not thousands of sophisticated structures built with luminescent divalent ruthenium complexes have been designed and tested so far.[19–24] The main reason for this sidelining can be found in the Cr^{III} coordination chemistry, which somehow mirrors that of trivalent cobalt with the formation of kinetically inert complexes as exemplified by the very small rate constants found for ligand exchange (*e.g.*, $k_{H_2O} = 2.4 \times 10^{-6}$ s^{-1} for $[Cr(H_2O)_6]^{3+}$)[25] and for hydrolysis (*e.g.*, $k_{hydrolysis} = 3.5 \times 10^{-4}$ s^{-1} for *cis*-$[Cr(ethylenediamine)_2Cl_2]^+$ under acidic conditions).[26] Consequently, Cr^{III} cannot be part of sophisticated multi-component self-assembly processes, in which structural self-healing under thermodynamic control is crucial.[27] Some rare (but remarkable) exceptions arose with (i) the serendipitous crystallization by Winpenny and coworkers of poly-chromium wheels at high temperatures (210 °C to 400 °C) using thermally resistant ligands[28–30] and (ii) the use of preformed chromium complexes working as inert partners for the preparation of hydroxo,[31] oxalato,[32,33–36] and cyano bridged architectures.[7,9,37] In this context, post-modifications were recently shown to open novel pathways for the stepwise building of multi-metallic assemblies including inert ruthenium–polypyridine complexes[38–40] or platinum–salen derivatives,[41,42] but the manipulation of related Cr^{III}–polypyridine entities remains scarce and elusive.[43–45] Moreover, recent demonstration that $[Cr(2,2':6',2''\text{-terpyridine})_2]^{3+}$ ($\equiv[Cr(tpy)_2]^{3+}$) complexes rapidly dissociate under slightly alkaline conditions,[46] a trend which confirms a previous observation reported for $[Cr(2,2'\text{-bipyridine})_3]^{3+}$ ($\equiv[Cr(bpy)_3]^{3+}$),[47] prevents post-treatment of these complexes for the design of organized polynuclear assemblies. To the best of our knowledge, trivalent chromium has thus never been used as a partner for thermodynamic multi-component self-assembly processes occurring in solution, but its labile divalent precursor Cr^{II} was shown to successfully promote the synthesis of heterometallic d–f triple-

[a]*Department of Inorganic and Analytical Chemistry, University of Geneva, 30 quai E. Ansermet, CH-1211 Geneva 4, Switzerland. E-mail: Benjamin.Doistau@unige.ch, Claude.Piguet@unige.ch*
[b]*Laboratory of Crystallography, University of Geneva, 24 quai E. Ansermet, CH-1211 Geneva 4, Switzerland*
[c]*Department of Physical Chemistry, University of Geneva, 30 quai E. Ansermet, CH-1211 Geneva 4, Switzerland. E-mail: Andreas.Hauser@unige.ch*

†Electronic supplementary information (ESI) available. CCDC 1542315–1542329. For ESI and crystallographic data in CIF or other electronic format see DOI: 10.1039/c7dt01747b

‡These authors contributed equally to this research work.

stranded helicates under thermodynamic control.[48,49] Subsequent air oxidation led to inert luminescent Cr^{III} sensitizers, which induced unprecedented lanthanide-centred molecular energy-transfer upconversion.[50–53] Last but not least, the characterization of Cr^{III} complexes in solution is severely hampered by the broad and poorly interpretable NMR signals produced by the long electronic relaxation times (about 0.5 ns) of their zero-field split $Cr(^4A_2)$ ground state.[54] This drawback is overcome for diamagnetic Ru^{II} complexes, which were thus selected for building well-defined photoactive polynuclear architectures useful for water splitting,[55] light-harvesting and energy conversion.[56–58] Nevertheless, while trivalent chromium exhibits some shortcomings compared to divalent ruthenium, its photophysical properties in pseudo-octahedral complexes offer some unparalleled attractiveness since the visible window is dominated by a single spin-allowed absorption band corresponding to the $Cr(^4T_2 \leftarrow {}^4A_2)$ transition, the energy of which can be easily tuned by the ligand-field parameter Δ, whereas the near-infrared window is governed by efficient long-lived $Cr(^2E \leftarrow {}^4A_2)$ phosphorescence, the energy of which is controlled by the nephelauxetic effect tuned by the Racah parameters B and C (Fig. 1).[13,59,60] It is thus trivial to switch from low-energy absorption combined with high-energy phosphorescence found in CrO_6 chromophores (small values of Δ and large values of B) toward the opposite situation found in CrN_6 chromophores.[13] Furthermore, the almost spin-only behavior combined with negligible zero-field splitting parameters measured for the degenerate paramagnetic $Cr(^4A_2)$ ground state (for instance D = 0.03 cm^{-1} for $[(tpy)CrCl_3]$)[61] offers a simple approach for unravelling electronic intermetallic communications *via* the estimation of the isotropic exchange coupling constant operating between chromium centres.[10,12,62]

In diamagnetic polynuclear Ru^{II} architectures, for which the Creutz–Taube complex is the archetype (Fig. 2a),[63] the magnitude of the intermetallic interaction is deduced from the envelope of the intervalence electronic absorption bands occurring in mixed valence Ru^{II}–Ru^{III} dimers.[64–68] When applied to back-to-back bis-terpyridine bridging ligands L in $[(tpy)Ru(L)Ru(tpy)]^{5+}$ (Fig. 2b), the associated theories successfully rationalized the exponential decrease of the electronic interaction parameter with increasing intermetallic separations[69–71] and the magnification of both through-bond electron transfer (Fig. 2c)[72,73] and energy transfer (Fig. 2d)[74–78] for short electron-rich aromatic bridges. Unfortunately, one-electron reductions of $[Cr(bpy)_3]^{3+}$ and $[Cr(tpy)_2]^{3+}$ occur on the bound ligands[79,80] and no related approach can be envisioned for unravelling intermetallic coupling in analogous polypyridine Cr^{III} complexes.

Altogether, the magnetic and photophysical properties of Ru^{II} polypyridine and Cr^{III} polypyridine complexes are complementary, with each series displaying specific advantages and shortcomings, but the paramagnetism associated with the three unpaired electrons in Cr^{III} opens additional perspectives. However, the lack of easy accessible synthetic procedures for the preparation and characterization of pure heteroleptic polynuclear chromium complexes has up to now prevented Cr^{III} polypyridines from being used as active building blocks in (supra)molecular optical devices. Recently, Barker *et al.*,[81] Isaacs *et al.*[82] and Housecroft and Constable *et al.*[46,83,84] tried to find a remedy for this frustrating limitation with the systematic exploration of the stability and lability of mononuclear

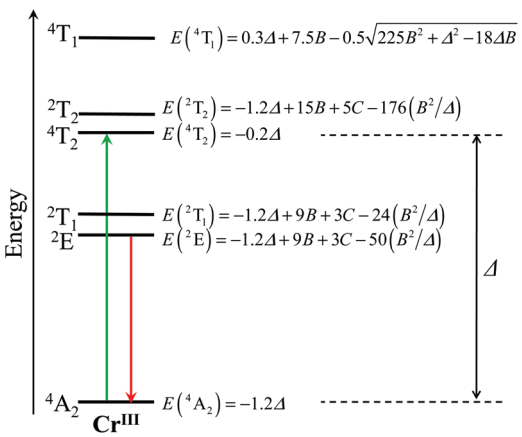

Fig. 1 Low-energy part of the energy level diagram for an octahedral Cr^{III} sensitizer showing the energy levels modeled in terms of the ligand field strength Δ and the Racah parameters B and C.[59,60] The upward green arrow stands for the lowest-energy spin-allowed absorption transition, while the downward red arrow refers to the lowest-energy phosphorescence.

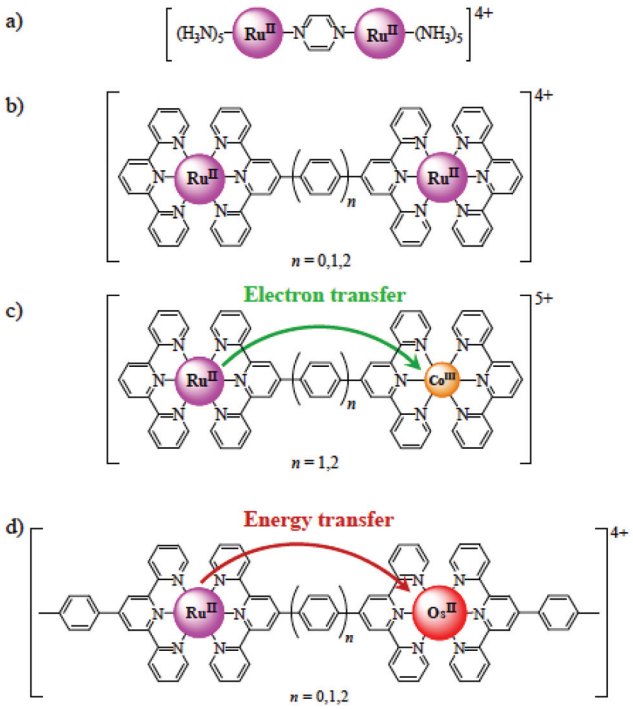

Fig. 2 (a) Creutz–Taube complex, (b) $[(tpy)Ru(L)Ru(tpy)]^{m+}$ complexes,[69–71] (c) $[(tpy)Ru^{II}(L)Co^{III}(tpy)]^{5+}$ complexes displaying directional electron transfer,[72,73] (d) $[(tpy)Ru^{II}(L)Os^{II}(tpy)]^{4+}$ complexes displaying directional energy transfer.[74,75]

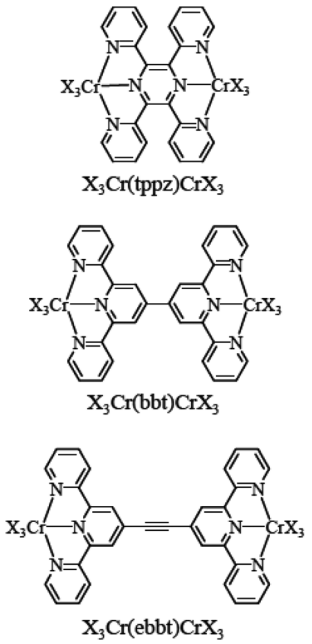

Scheme 1 Structures and nomenclature of the investigated dinuclear chromium complexes. tppz = 2,3,5,6-tetra-2-pyridinylpyrazine, bbt = 4,4‴-bis(2,2′:6′,2″-terpyridine), and ebbt = 4,4‴-(ethynyl)-bis(2,2′:6′,2″-terpyridine). X_3 stands for Cl_3 or 2,2′:6′,2″-terpyridine.

six-coordinate bis-terimine[83,84] and ter-bisimine[46,81,82] Cr^{III} complexes. Building on the identification of labile Cr^{III}–O(triflate) bonds and their easy formation from Cr–Cl bonds, we herein propose to extend this procedure for the synthesis of a series of novel back-to-back dinuclear $[X_3Cr^{III}(L)Cr^{III}X_3]$ complexes (Scheme 1, $X_3 = Cl_3$ or X_3 = tpy), which are reminiscent of the well-known Ru^{II} dyads. We also plan to unravel the intermetallic electronic communication with the help of magnetic measurements (isotropic superexchange coupling constants), photophysical studies (ligand-field and Racah parameters and intermetallic energy transfer rate constants) and thermodynamic considerations (cooperative binding of labile Er^{3+} as a model for Cr^{3+}).

Results and discussion

Synthesis and characterization of homoleptic and heteroleptic mononuclear $[CrLCl_3]$, $[CrL_2](PF_6)_3$ (L = tpy, ebzpy, tppz) and dinuclear $[Cl_3Cr(L)CrCl_3]$, $[(tpy)Cr(L)Cr(tpy)](PF_6)_6$ (L = tppz, bbt, ebbt) complexes

As a first step toward this goal, we used Ga^{III} as a trivalent labile diamagnetic model cation for Cr^{III} for the straightforward formation of a homoleptic $[Ga(tpy)_2]^{3+}$ cation (Table S1, ESI†), which displayed the expected well-resolved D_{2d}-symmetrical ^1H NMR spectrum (6 signals observed for 22 available aromatic protons, Fig. S1, ESI†). The downfield shifts of the aromatic signal ($\Delta\delta$ = −1.01 ppm) observed for the hydrogen nuclei located at the *ortho*-positions of the nitrogen atoms of the distal pyridine rings are diagnostic for an orthogonal arrangement of the two planar tridentate terpyridine ligands around the central cation as found in $[Fe(tpy)_2]^{2+}$ ($\Delta\delta$ = −1.64 ppm), $[Ru(tpy)_2]^{2+}$ ($\Delta\delta$ = −1.37 ppm) and $[Os(tpy)_2]^{2+}$ ($\Delta\delta$ = −1.43 ppm).[85] The crystal structure of $[Ga(tpy)_2](PF_6)_3{\cdot}2CH_3CN$ (**1**, Fig. 3 left, Fig. S2 and Tables S2, S4 and S5†) confirmed this statement with an interplanar angle of 88.5° between the two tridentate N_3 chelates. Combined with the pincer effect brought by the two-fused 5-membered chelate rings in the terpyridine moieties (N_{distal}–Cr–N_{distal} = 156.6(1)° instead of 180° expected for octahedral geometry, see Fig. 3), the diamagnetic GaN_6 core adopts the expected compact and slightly distorted pseudo-octahedral geometry previously reported for other $[M(tpy)_2]^{z+}$ (z = 2, 3) complexes.[86,87] No specific close-packing interactions due to significant π–π aromatic interactions compatible with 'terpyridine embrace' supramolecular patterns[87] could be identified (the closest inter-aromatic distance amounts to 4.5 Å, far beyond the accepted cutoff of 3.8 Å for π-stacking interactions; Fig. S3†).[88,89] We however note that $[Ga(tpy)_2](PF_6)_3{\cdot}2CH_3CN$ (**1**) crystallizes in the chiral $P2_12_12_1$ space group, the origin of which probably arises from packing effects since $[Ga(tpy)_2]^{3+}$ cations are essentially achiral. In order to overcome the complications produced by the kinetic inertness of Cr^{III} salts, the related homoleptic complex $[Cr(tpy)_2]^{3+}$ is obtained by the reaction of the reduced labile precursor $Cr(CF_3SO_3)_2{\cdot}H_2O$[48] with 2,2′:6′,2″-terpyridine (tpy), or with its extended analogue 2,6-bis(1-ethyl-benzimidazol-2-yl)pyridine (ebzpy),[90] to give saturated six-coordinated Cr^{II} complexes.[80] Subsequent air oxidation (outer sphere mechanism)[48] provides $[Cr(tpy)_2](PF_6)_3{\cdot}2.5CH_3CN$ (**2**, Fig. S4 and Tables S2, S6 and S7, ESI†) and $[Cr(ebzpy)_2](PF_6)_3{\cdot}5.5CH_3CN$ (**3**, Fig. S5 and Tables S3, S8–S11, ESI†) in 70–80% yields after metathesis with PF_6^- (Fig. 3).

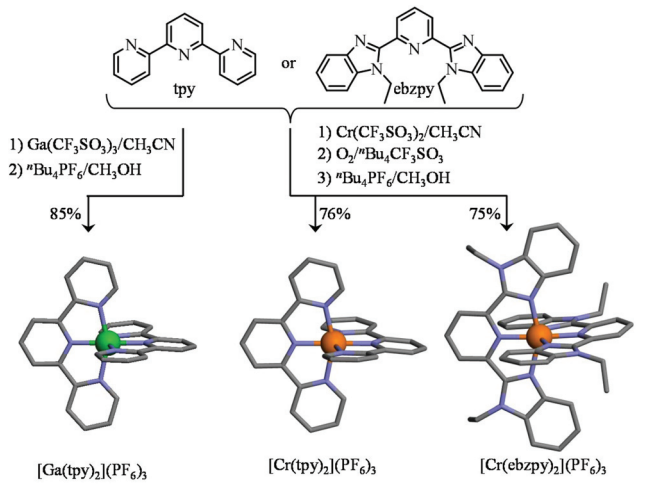

Fig. 3 Synthesis of the homoleptic tricationic $[Ga(tpy)_2]^{3+}$ $[Cr(tpy)_2]^{3+}$ and $[Cr(ebzpy)_2]^{3+}$ complexes. The molecular structures of the cations are those found in the crystal structures of $[Ga(tpy)_2](PF_6)_3{\cdot}2CH_3CN$ (**1**), $[Cr(tpy)_2](PF_6)_3{\cdot}2.5CH_3CN$ (**2**) and $[Cr(ebzpy)_2](PF_6)_3{\cdot}5.5CH_3CN$ (**3**). The hydrogen atoms have been omitted for clarity. Color code: C = grey, N = blue, Cr = orange, Ga = green.

The molecular structures of the CrN_6 (**2** and **3**) and GaN_6 (**1**) moieties are almost superimposable and closely match that previously reported for $[Cr(tpy)_2](ClO_4)_3{\cdot}H_2O$.[91,92] Again, intermolecular packing interactions are very limited for these chromium complexes (Fig. S6 and S7, ESI†), a trend assigned to the combination of (i) the considerable inter-cation repulsions and (ii) the delicate accommodation of three counter-anions per cationic complex in the crystal structures.[46] We would like to stress here that the crystal structure of **2**, monitored at 180 K in this work, is identical to that previously deposited for $2\{[Cr(tpy)_2](PF_6)_3\}{\cdot}5CH_3CN$ recorded at 123 K,[46] an observation which confirms the robustness of the packing process despite the lack of identifiable strong intermolecular interactions in the crystal structures of these $[Cr(tpy)_2]X_2$ complexes.

Since no high-resolution NMR signals could be recorded for the slow-relaxing Cr^{III} complexes, their magnetic characterization in solution is restricted to the measurement of the effective magnetic moments in acetonitrile for $[Cr(tpy)_2](PF_6)_3$ (μ_{eff} = 4.4(4) BM) and $[Cr(ebzpy)_2](PF_6)_3$ (μ_{eff} = 4.2(4) BM), which only slightly deviate from the spin-only value (μ_{eff} = 3.88 BM). Unfortunately, we were not able to record satisfying ESI-MS spectra for these mononuclear triply-charged complexes in solution, probably because of partial dissociation occurring during the vaporization process.[46]

Higher structural complexity requires the rational synthesis of heteroleptic bis-terdentate CrN_6 chromophores following the strategy originally proposed by Barker *et al.* for bidentate phenanthroline ligands[81] and adapted for tridentate terpyridines by Housecroft and Constable and coworkers (Fig. 4).[46,84] Beyond $[Cr(tpy)Cl_3]$, the structure of which was previously reported (Fig. 4 top centre),[61,93] we confirm that the three weakly bound THF molecules in $CrCl_3(THF)_3$ can be displaced by closely related tridentate ligands[94] to give $[Cr(ebzpy)Cl_3]{\cdot}DMF$ (**5**, Tables S12–S14 and Fig. S8 and S9†) and $[Cr(tppz)Cl_3]{\cdot}2DMF$ (**6**, Tables S12, S15, and S16 and Fig. S8 and S9†).[95] The three CrN_3 chelate units are almost superimposable showing similar bond distances (Cr–N = 2.05(3) Å) and bond angles (average pincer angle N_{distal}–Cr–N_{distal} = 156.5 (5)°). The crystal structure of $[Cr(tppz)Cl_3]$ (**6**) reveals specific geometric distortions at the metal centre caused by the repulsion of the hydrogen atoms at the 3-position of the bound pyridine rings with the two unbound pyridine units. The result is a twisting of the bound part of the tppz ligand, in which the dihedral angles between the pyridine and pyrazine rings amount to 19.46°. The reaction of $[Cr(L)Cl_3]$ with concentrated trifluoromethanesulfonic acid (CF_3SO_3H) displaces the three chloride anions to give $[Cr(L)(CF_3SO_3)_3]$ (L = tpy, ttpz, Table S1†). The slightly more basic ebzpy ligand (compared with tpy and ttpz) did not resist protonation and only $[H_2ebzpy](CF_3SO_3)_2$ could be isolated (**10**, Fig. S10 and Tables S17 and S18†). Subsequent mixing of $[Cr(L)(CF_3SO_3)_3]$ with a second tridentate ligand L′ either restores the homoleptic complexes (L′ = L) or provides (L′ ≠ L) the heteroleptic complexes $[Cr(tpy)(ebzpy)](PF_6)_3$ (**7**, Fig. S11 and Tables S17, S19 and S20†) and $[Cr(tpy)(tppz)](PF_6)_3$ (**8**, Fig. S12 and Tables S21–S25†) in fair to good yields (Fig. 4 bottom). Their molecular

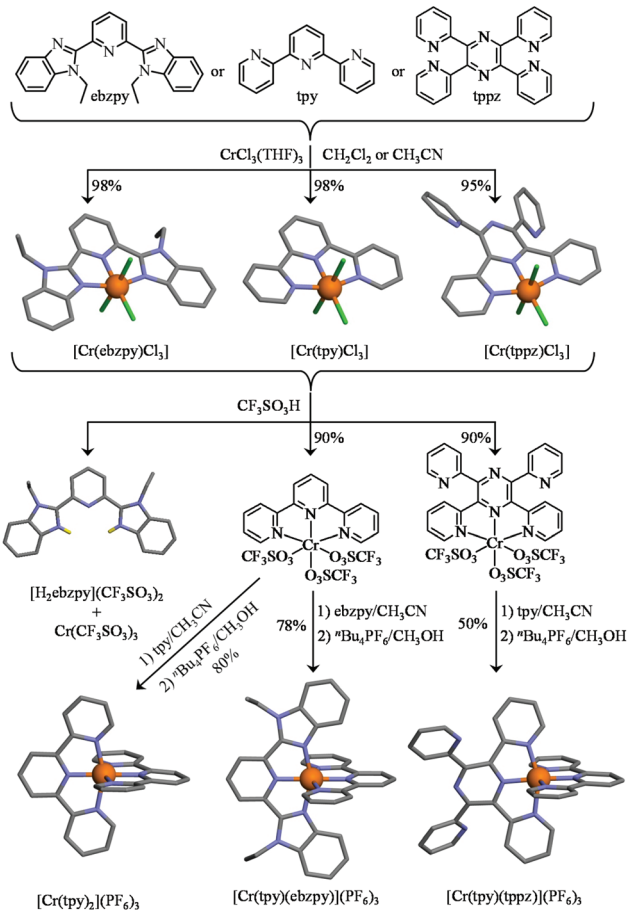

Fig. 4 Synthesis of the heteroleptic mononuclear chromium complexes. The molecular structures are those found in the crystal structures of $[Cr(ebzpy)Cl_3]{\cdot}DMF$ (**5**), $[Cr(tpy)Cl_3]{\cdot}(CH_3)_2SO$,[93] $[Cr(tppz)Cl_3]{\cdot}2DMF$ (**6**) $[Cr(tpy)_2](PF_6)_3{\cdot}2.5CH_3CN$ (**2**), $[Cr(tpy)(ebzpy)](PF_6)_3{\cdot}2CH_3CN$ (**7**), $[Cr(tpy)(tppz)](PF_6)_3{\cdot}3CH_3CN$ (**8**) and $[H_2(ebzpy)](CF_3SO_3)_2$ (**10**). The hydrogen atoms have been omitted for clarity. Color code: C = grey, N = blue, Cr = orange, Cl = green, H = yellow.

structures show CrN_6 units almost superimposable with those found in the homoleptic model cations $[Cr(tpy)_2]^{3+}$ and $[Cr(ebzpy)_2]^{3+}$. Again, no remarkable intermolecular π-stacking interactions could be highlighted (Fig. S13 and S14†) and the structural distortion produced by steric congestion with the non-coordinated pyridine rings in the tppz ligand is retained in $[Cr(tpy)(tppz)]^{3+}$ (the average dihedral angle between the pyridine and pyrazine rings in the tridentate bound unit amounts to 19(4)°).

With this strategy at hand, the synthesis of a series of six rod-like heteroleptic dinuclear Cr^{III} complexes with three different bridging ligands (tppz, bbt, and ebbt) and two types of capping entities (Cl_3 or tpy) can be envisioned. Firstly, the reaction of an excess of $CrCl_3{\cdot}6H_2O$ with the appropriate bridging ligand[95] quantitatively yields $[Cr_2Cl_6(tppz)]$ and $[Cr_2Cl_6(bbt)]$, while $[Cr_2Cl_6(ebbt)]$ is obtained with more difficulties because of the low solubility of the free ligand in common organic solvents (left part of Fig. 5 and Table S1†).

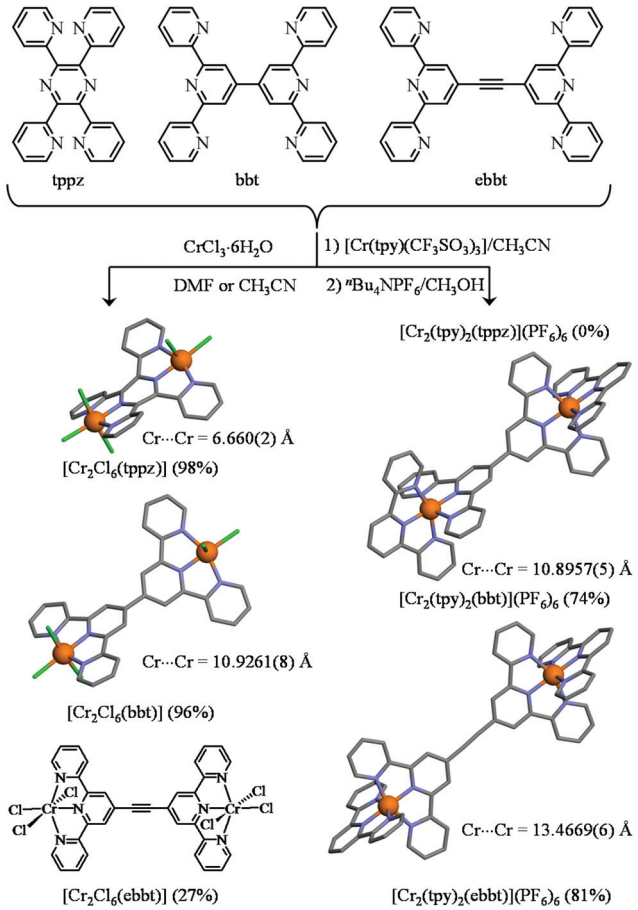

Fig. 5 Synthesis of the heteroleptic dinuclear chromium complexes. The molecular structures are those found in the crystal structures of $[Cr_2Cl_6(tppz)]\cdot 3C_5H_9NO$ (**11**), $[Cr_2Cl_6(bbt)]$ (**12**), $[Cr_2(tpy)_2(bbt)](PF_6)_6\cdot 8CH_3CN\cdot(CH_3CH_2)_2O$ (**13**) and $[Cr_2(tpy)_2(ebbt)](PF_6)_6\cdot 10CH_3CN$ (**14**). The hydrogen atoms have been omitted for clarity. Color code: C = grey, N = blue, Cr = orange, Cl = green.

Alternatively, stoichiometric reactions between the bridging ligand (1 eq.) and labile $[Cr(tpy)(CF_3SO_3)_3]$ (2 eq.) lead to the targeted dinuclear complexes $[Cr_2(tpy)_2(bbt)](PF_6)_6$ and $[Cr_2(tpy)_2(ebbt)](PF_6)_6$, but we were unable to connect two triply charged $[Cr(tpy)]^{3+}$ cations at the termini of the shorter tppz ligand (Fig. 5). The crystal structure of $[Cr_2Cl_6(tppz)]\cdot 3C_5H_9NO$ (**11**, Fig. S15 and Tables S26–S28†), with its intermetallic distance 6.662(3) Å and interplanar angle of 25.5° between the two chelate N_3 planes, completes a collection of similar rod-like dyads reported for $[Ru_2Cl_6(tppz)]^-$ ($Ru^{II}\cdots Ru^{III}$ = 6.504 Å, interplanar angle = 26.38°),[96] $[Ru_2(CH_3CN)_6(tppz)]$ ($Ru^{II}\cdots Ru^{II}$ = 6.56 Å, interplanar angle = 27.08°)[97] and for other $[M_2X_6(tppz)]$ binuclear complexes.[98–102] The crystal structures involving the extended bbt bridging ligands $[Cr_2Cl_6(bbt)]$ (**12**, Fig. S16 and Tables S26, S29 and S30†) and $[Cr_2(tpy)_2(bbt)](PF_6)_6\cdot 8CH_3CN\cdot(CH_3CH_2)_2O$ (**13**, Fig. S17 and Tables S31–S33†) have surprisingly no precedent for analogous ruthenium complexes despite the intense activity dedicated to these specific supramolecular architectures.[19–24,69] The intermetallic separation is fixed to *ca.* 10.9 Å by the back-to-back bis(terpyridine) spacer (Fig. 5). The dihedral angle within the bridging 4,4′-bipyridine motif amounts to 36.5(4)° in $[Cr_2Cl_6(bbt)]$ and to 83.0(1)° in $[Cr_2(tpy)_2(bbt)](PF_6)_6$. While the smaller angle matches the theoretically computed interplanar angle of 35–40°, which simultaneously minimizes the torsion energy and optimizes orbital overlap in 4,4′-bipyridine,[103–105] the almost orthogonal arrangement of the two central pyridine rings found in $[Cr_2(tpy)_2(bbt)](PF_6)_6$ is unique for this spacer since the largest value reported so far reached 61(1)° for a dinuclear copper(II) complex.[106] Four PF_6^- counter-anions are located between the two CrN_6 units of the dinuclear complex. They are involved in twelve $C_{aromatic}$–H···F–P hydrogen bonds (2.4 Å to 2.6 Å),[107,108] which significantly stabilize the orthogonal arrangement of the central back-to-back bis(terpyridine) spacer (Fig. S18†). The crystal structure of $[Cr_2(tpy)_2(ebbt)](PF_6)_6\cdot 10CH_3CN$ (**14**, Fig. S19 and Tables S31, S34 and S35†) obviously displays not only the longest intramolecular Cr···Cr distance (13.4669(6) Å, Fig. 5), but also the smallest dihedral angle between the two quasi-planar terpyridine units connected by the alkyne bridge (0.1(3)°). To the best of our knowledge, no molecular structure has been previously reported with this extended ebbt ligand.[109] We are now in a position to investigate the nature and magnitude of intramolecular intermetallic interactions operating between pseudo-octahedral Cr^{III} metallic cations incorporated into rod-like heteroleptic dyads possessing variable lengths.

Unravelling intermetallic communication in dinuclear $[Cl_3Cr(L)CrCl_3]$, $[(tpy)Cr(L)Cr(tpy)](PF_6)_6$ complexes (L = tppz, bbt, ebbt): magnetic evidence

Two trivalent Cr^{III} centres connected by short oxide bridges usually display strong anti-ferromagnetic interaction ($J_{ex} < 0$) operating between the two $S = 3/2$ spin carriers *via* a super-exchange mechanism.[62] Application of the van Vleck equation to a coupled Cr^{III} pair obeying the Heisenberg–Dirac–van Vleck spin Hamiltonian $\hat{H}_{HDVV} = -J_{ex}\hat{S}_A\hat{S}_B$ ($\hat{S}_A$ and $\hat{S}_B$ are the spin operators localized on each metallic centre and J_{ex} is the phenomenological magnetic exchange coupling constant) provides a contribution to the paramagnetic susceptibility χ_{para}^{dimer} expressed in eqn (1), where g is the Landé factor, $N_A = 6.022 \times 10^{23}$ mol^{-1} is Avogadro's number, $\mu_B = 9.274 \times 10^{-24}$ J T^{-1} is the Bohr magneton and $k_B = 1.3806 \times 10^{-23}$ J K^{-1} is the Boltzmann constant.[62]

$$\chi_{para}^{dimer} = \frac{N_A g^2 \mu_B{}^2}{k_B T} \frac{2e^{J_{ex}/k_B T} + 10e^{3J_{ex}/k_B T} + 28e^{6J_{ex}/k_B T}}{1 + 3e^{J_{ex}/k_B T} + 5e^{3J_{ex}/k_B T} + 7e^{6J_{ex}/k_B T}} \quad (1)$$

Compared with $|J_{ex}|$ values expected in the 1–10 cm^{-1} range for the $[X_3Cr(L)CrX_3]$ dyads, the weak contribution of the zero-field splitting (D = 0.03 cm^{-1} for $[Cr(tpy)Cl_3]$, D = 0.2 cm^{-1} for $[Cr(tpy)_2]^{3+}$)[12,61,80] can be neglected and the magnetic susceptibilities recorded in the 2–300 K range for the five dimeric complexes (Fig. 6 plotted as χT *vs.* T) could be satisfyingly fitted to eqn (2), where χ_{para}^{dimer} is given in eqn (1), χ_{dia}^{dimer} is the diamag-

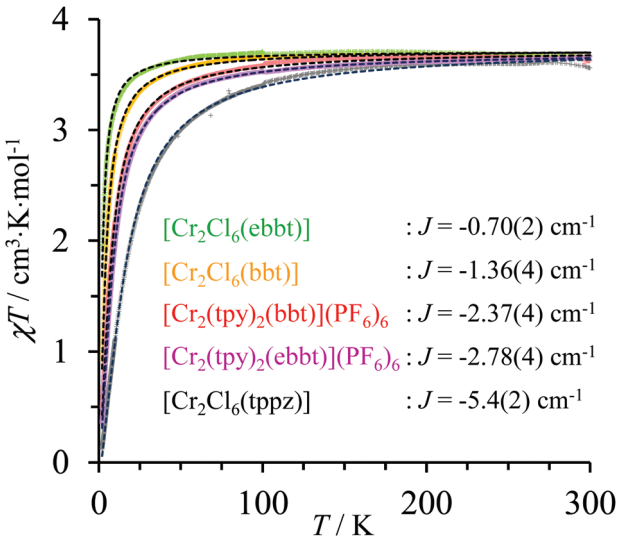

Fig. 6 Dependence of $\chi_{tot}^{dimer}T$ on the applied temperature (2–300 K) for the dinuclear Cr^{III} complexes showing the experimental data (colored crosses) and non-linear least-square fits with eqn (2) (black dotted traces).

netic susceptibility of the dimer calculated by means of Pascal's constant[110] and χ_{TIP}^{dimer} is the temperature-independent paramagnetic contribution of the dimer (Table S36†).

$$\chi_{tot}^{dimer} = \chi_{para}^{dimer} + \chi_{dia}^{dimer} + \chi_{TIP}^{dimer} \quad (2)$$

For temperatures larger than 150 K, the magnetic susceptibilities of all dinuclear complexes converge to a common constant value of $3.55 \leq \chi T \leq 3.67$ cm^3 mol^{-1}, which is close to χT = 3.75 cm^3 mol^{-1} calculated for two independent spin-only Cr^{III} centres (S = 3/2). At low temperature, the χT *versus* T curves abruptly decrease, which is diagnostic for weak intramolecular anti-ferromagnetic interactions, the magnitude of which can be estimated by the exchange constants $-5.4 \leq J_{ex} \leq -0.7$ cm^{-1} collected in Fig. 6 (Table S36†). The J_{ex} values found for pairs of coupled CrN_3Cl_3 units in dinuclear $[Cl_3Cr(L)CrCl_3]$ dyads (orange, green and black traces in Fig. 6) show the expected reduction of the efficiency of the anti-ferromagnetic superexchange pathway with the increasing length of the molecular bridge separating the paramagnetic Cr^{III} centres ($J_{ex}^{tppz} < J_{ex}^{bbt} < J_{ex}^{ebbt}$). Switching from $CrCl_3N_3$ to CrN_6 coordination spheres in going from $[Cl_3Cr(bbt)CrCl_3]$ (J_{ex} = −1.36 cm^{-1}, orange trace) to $[(tpy)Cr(bbt)Cr(tpy)]^{6+}$ (J_{ex} = −2.37 cm^{-1}, red trace) is accompanied by an almost doubling of the magnitude of the anti-ferromagnetic exchange interactions for a fixed intermetallic distance of 10.9 Å (Fig. 5 and Table S36†). This trend is particularly counter-intuitive since the largest anti-ferromagnetic communication is found for $[(tpy)Cr(bbt)Cr(tpy)]^{6+}$, in which the dihedral angle between the connected pyridine rings of the 4,4′-bipyridine bridge is close to 90° thus minimizing π-orbital overlap.[111,112] We however note that related trends, previously observed for oxo bridged Cr^{III} binuclear complexes, could be assigned to the relative energies of the natural magnetic orbitals (t_{2g} for a pseudo-octahedral Cr^{III} complex) with respect to that of the HOMO orbital of the bridging ligand.[113] Applying this reasoning to the replacement of three anionic π-donor chloride ligands in $[Cl_3Cr(bbt)CrCl_3]$ with three π-acceptor heterocyclic nitrogen atoms in the capping terpyridine units in $[(tpy)Cr(bbt)Cr(tpy)]^{6+}$ is expected to decrease the energy of the Cr-centred pseudo-t_{2g} magnetic orbitals, thus favoring their mixing with the occupied molecular orbitals of the back-to-back bis(terpyridine) bridge. A thorough theoretical approach dealing with Fe^{III}–Cu^{II} complexes recently confirmed the prospective dependence of the exchange interaction constant with the nature of the ligand field.[114] Finally, the *a priori* surprising increase of the anti-ferromagnetic interaction accompanying the 24% increase of the intermetallic distance on going from $[(tpy)Cr(bbt)Cr(tpy)]^{6+}$ (Cr···Cr = 10.9 Å, J_{ex} = −2.37 cm^{-1}, red trace) to $[(tpy)Cr(ebbt)Cr(tpy)]^{6+}$ (Cr···Cr = 13.5 Å, J_{ex} = −2.78 cm^{-1}, violet trace) can be assigned to the beneficial effect of the bridging alkyne unit, which reduces the dihedral angle between the connected pyridine rings from 83.2(3)° in the bbt spacer to 0.1(3)° in the ebbt analogue and thus favors the overlap integral leading to detectable intramolecular anti-ferromagnetic interactions on the nanometric scale.

Unravelling intermetallic communication in dinuclear $[Cl_3Cr(L)CrCl_3]$, $[(tpy)Cr(L)Cr(tpy)](PF_6)_6$ complexes (L = tppz, bbt, ebbt): optical evidence

The experimental energies of the Cr^{III}-centred excited states (with respect to that of the $Cr(^4A_2)$ ground state) are deduced from the combination of the absorption (Fig. 7a and b and Appendix 1 in the ESI†) and emission (Fig. 7c and Appendix 2 in the ESI†) spectra recorded for the dinuclear complexes in solution and in the solid state (Table 1 columns 7–9). At first sight, the energy of these levels can be roughly modeled by using the diagonal elements of the Tanabe–Sugano matrices assuming a pseudo-octahedral geometry for the CrN_3Cl_3 and CrN_6 chromophores found in $[Cl_3Cr(L)CrCl_3]$ (L = tppz, bbt, ebbt) and $[(tpy)Cr(L)Cr(tpy)](PF_6)_6$ (L = bbt, ebbt).[115] However, this level of approximation implies that the $Cr(^2E)$ and $Cr(^2T_1)$ states are degenerate, which is clearly not the case in these dimeric complexes (Fig. 7 and Table 1).

The additional consideration of configuration interaction between the states of the same multiplicity and symmetry, but from different strong field configurations led Jorgensen[59] to introduce second-order corrections $\alpha B^2/\Delta$ in eqn (3)–(5), which are derived from the off-diagonal elements of the Tanabe–Sugano matrices.

$$E(^4T_2) = \Delta \quad (3)$$

$$E(^2T_1) = 9B + 3C - 24(B^2/\Delta) \quad (4)$$

$$E(^2E) = 9B + 3C - 90(B^2/\Delta) \quad (5)$$

Although Jorgensen[59] fixed C/B = 4 for deriving eqn (3)–(5), there is no obvious reason for this assumption and a systematic and detailed ligand-field analysis of electronic spectra

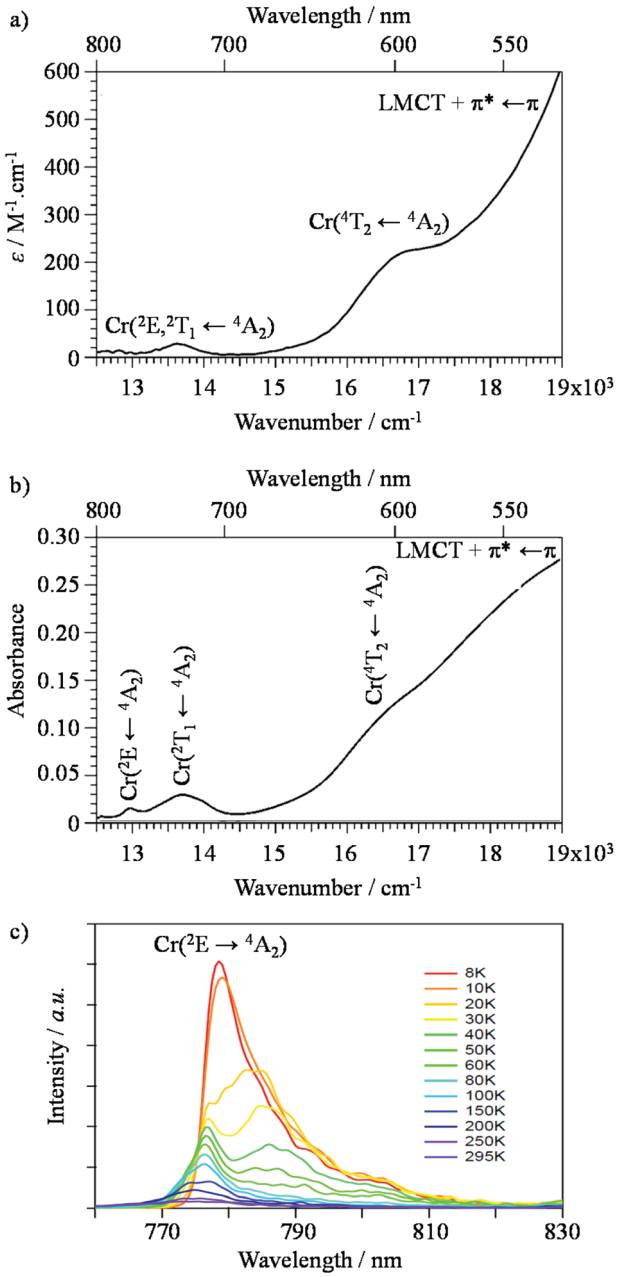

Fig. 7 Absorption spectra recorded for [(tpy)Cr(bbt)Cr(tpy)](PF$_6$)$_6$ (a) in acetonitrile solution (2.5 × 10^{-5} mol dm^{-3}, 295 K) and (b) in the solid state. (c) Corresponding solid state emission spectra collected at variable temperatures (λ_{exc} = 400 nm).

recorded for Cr^{III} compounds revealed that $3 \leq C/B \leq 8$.[115] In his seminal textbook,[60] Lever replaced eqn (5) with eqn (6).

$$E(^2\mathrm{E}) = 9B + 3C - 50(B^2/\Delta) \quad (6)$$

This transforms the modelling of the $E(^2T_1) - E(^2E)$ energy gap, for which Jorgensen's approach predicts $66B^2/\Delta$ (eqn (5)), to only $26B^2/\Delta$ (eqn (6)). Compared with the theoretical set of exact energies computed by Ferguson by means of full Eisenstein's matrices with B = 680 cm^{-1} and C = 2720 cm^{-1} (C/B = 4.0),[116,117] the exact computed $E(^2T_1) - E(^2E)$ energy gap amounts to 630 cm^{-1} for Δ = 19 940 cm^{-1} in fair to good agreement with the prediction of the second-order correction $26B^2/\Delta$ = 603 cm^{-1} (eqn (6)), but rather far from 1531 cm^{-1} obtained with eqn (5). We conclude that only a complete ligand-field treatment is capable of extracting reliable Racah parameters B and C for Cr^{III} complexes,[119] but eqn (6) seems superior to eqn (5) when a rough modeling of the energy of the lowest spin–flip ^{2}E excited state is foreseen. We therefore used eqn (3), (4) and (6) for estimating the ligand-field strength Δ and the Racah parameters B and C for each dimeric and monomeric complex (Table 1 and Fig. 8, Table S37 and Fig. S20 in the ESI†) together with eqn (7) and (8) for predicting the energy of the missing Cr(^{2}T$_2$) and Cr(^{4}T$_1$) levels.

$$E(^2T_2) = 15B + 5C - 176(B^2/\Delta) \quad (7)$$

$$E(^4T_1) = 1.5\Delta + 7.5B - 0.5\sqrt{225B^2 + \Delta^2 - 18B\Delta} \quad (8)$$

In agreement with both the spectrochemical and the nephelauxetic series,[118] the ligand-field parameters in mononuclear complexes increase on going from CrN_3Cl_3 (16 300 ≤ Δ ≤ 17 000 cm^{-1}) to CrN_6 (18 750 ≤ Δ ≤ 19 120 cm^{-1}), whereas the Racah parameters B = 682(19) cm^{-1} are comparable for both types of chromophores. A narrow distribution of these complexes around $\Delta/B \approx 25$ results in the d^3 Tanabe–Sugano diagram (Fig. S21†). The latter Δ/B values are significantly smaller than Δ/B = 31.2 reported for the well-known [Cr(bpy)$_3$](PF$_6$)$_3$ complex (Δ = 23 400 cm^{-1}, B = 730 cm^{-1} and C = 2730 cm^{-1}, C/B = 3.7)[119] because the pincer effect produced by 5-membered chelate rings operates four times in [Cr(L)$_2$]$^{3+}$ (L = tpy, ebzpy) and only three times in [Cr(bpy)$_3$]$^{3+}$. This deleterious effect is not a fatality for tridentate ligands and it can be overcome by the use of six-membered chelate rings as found in [Cr(ddpd)Cl$_3$] (**15**) (Fig. S22 and S23 and Tables S38–S40 in the ESI†) and in [Cr(ddpd)$_2$](BF$_4$)$_3$ complexes (ddpd = *N*,*N*′-dimethyl-*N*,*N*″-dipyridin-2-ylpyridine-2,6-diamine).[120] The larger N_{distal}–Cr–N_{distal} angle of 172.0(9)° observed in [Cr(ddpd)$_2$]$^{3+}$ (compared with 156.5(5)° in [Cr(tpy)$_2$]$^{3+}$) indeed restores a large ligand field strength in bis-terdentate pseudo-octahedral complexes (Δ = 22 990 cm^{-1}, Table S37†). Focusing now on the through-bridge effect produced by the connection of a second neutral $CrCl_3$ unit which transforms [Cr(tppz)Cl$_3$] into its dinuclear [Cl$_3$Cr(tppz)CrCl$_3$] analogue (Cr···Cr = 6.66 Å), we observe that Δ decreases by almost 500 cm^{-1} (Fig. 8). This effect can be taken as an assessment of the mutual polarization (*i.e.* electronic communication) produced by the two Cr^{III} centres connected to the bridging back-to-back bis-terdentate ligand. Taking now [Cr(tpy)Cl$_3$] as the mononuclear reference, the same trend is monitored for [Cl$_3$Cr(bbt)CrCl$_3$] (Δ decreases by 300 cm^{-1} for Cr···Cr = 10.93 Å) and [Cl$_3$Cr(ebbt)CrCl$_3$] (Δ decreases by 200 cm^{-1} for Cr···Cr ≥ 13 Å), but with an expected attenuation for longer intermetallic distances. For the charged [CrN_6]$^{3+}$ chromophore found in the mononuclear [Cr(tpy)$_2$]$^{3+}$ reference complex (Δ = 18 750 cm^{-1}, Table 1), the latter effect is drastically amplified leading to a *ca.* 2000 cm^{-1} reduction of the ligand-field parameter Δ in the

Table 1 Ligand-field energy Δ and Racah parameters (B and C) deduced with eqn (3), (4) and (6) by using the experimental energy of the excited $Cr(^2E)$, $Cr(^2T_1)$ and $Cr(^4T_2)$ levels observed for the dinuclear $[Cl_3Cr(L)CrCl_3]$ and $[(tpy)Cr(L)Cr(tpy)](PF_6)_6$ complexes (L = tppz, bbt, ebbt) and for their mononuclear analogues $[Cr(L)Cl_3]$ (L = tppz, tpy) and $[Cr(tpy)_2](PF_6)_3$

Compound	Δ/cm^{-1}	B/cm^{-1}	C/cm^{-1}	Δ/B	C/B	E/cm^{-1} [a] ^2E	$^2T_1$	$^4T_2$	$^2T_2$ [b]	$^4T_1$ [c]
$[Cr_2Cl_6(tppz)]$	16 000	708	2564	23	3.6	12 500	13 316	16 000	*17 927*	*22 893*
$[Cr_2Cl_6(bbt)]$	16 393	648	2785	25	4.3	12 903	13 569	16 393	*19 134*	21 980
$[Cr_2Cl_6(ebbt)]$	16 502	604	2863	27	4.7	12 920	13 495	16 502	*19 482*	*22 671*
$[Cr_2(tpy)_2(bbt)](PF_6)_6$	16 722	720	2636	23	3.7	12 837	13 643	16 722	*18 524*	*23 782*
$[Cr_2(tpy)_2(ebbt)](PF_6)_6$	16 474	668	2672	25	4[d]	12 674	*13 379*[d]	16 474	*18 614*	*23 132*
$[Cr(tppz)Cl_3]$	16 474	693	2770	24	4[d]	13 089	*13 846*[d]	16 474	*19 117*	*23 312*
$[Cr(tpy)Cl_3]$	16 694	697	2786	24	4[d]	13 175	*13 931*[d]	16 694	*19 265*	*23 585*
$[Cr(tpy)_2](PF_6)_3$	18 750	675	2698	28	4[d]	12 953	*13 584*[d]	18 750	*19 340*	*25 663*

[a] Energies are given with respect to that of the ground $Cr(^4A_2)$ level. [b] Computed with eqn (7). [c] Computed with eqn (8). [d] The $Cr(^2T_1 \leftarrow {}^4A_2)$ transition could not be unambiguously assigned and the associated Racah parameters were calculated assuming $C = 4B$. The energy of the $Cr(^2T_1)$ level was computed using eqn (4).

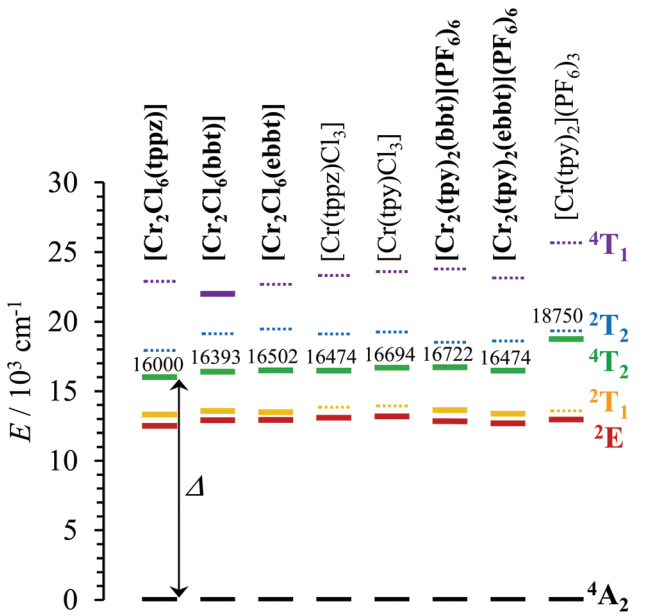

Fig. 8 Low-energy part of the energy level diagrams obtained for the dinuclear $[Cl_3Cr(L)CrCl_3]$ and $[(tpy)Cr(L)Cr(tpy)](PF_6)_6$ complexes (L = tppz, bbt, ebbt, bold font) and for their mononuclear analogues $[Cr(L)Cl_3]$ (L = tppz, tpy) and $[Cr(tpy)_2](PF_6)_3$ (normal font). The ligand-field Δ parameter is highlighted. Full traces are used for experimentally observed excited levels, whereas dotted traces correspond to calculated levels.

related charged dinuclear complexes $[(tpy)Cr(L)Cr(tpy)]^{6+}$ (L = bbt, ebbt, Fig. 8 and Table 1). The considerable reduction of Δ recorded for the longest ebbt bridging ligand in $[(tpy)Cr(ebbt)Cr(tpy)]^{6+}$ combined with the operation of the largest nephelauxetic dispersion (*i.e.* the minimum B Racah parameter, Table 1) confirms that an alternation of alkyne/aromatic groups is particularly adapted for the design of electronic wires between Cr^{III} centres, a result in line with the exceptional delocalization of the electronic density from the metal centres reported for analogous rod-like Ru(II)/Os(II) dyads.[121–123] Intermetallic communication can be alternatively probed by time-resolved emission spectroscopy performed on powder samples of the dinuclear complexes at cryogenic temperatures. The $Cr(^2E \rightarrow {}^4A_2)$ phosphorescence signals showed double exponential decays for all complexes except for the unsolvated centrosymmetrical $[Cr_2Cl_6(bbt)]$ complex, for which the kinetic decay trace is mono-exponential (Table 2 and Fig. A2-9–A2-13 in Appendix 2†).

Since (i) mono-exponential decay traces in the millisecond range are systematically recorded for the $Cr(^2E)$ phosphorescence occurring in related mononuclear chromium complexes ($0.24 \leq \tau_{Cr}(^2E) \leq 1.37$ ms at 3 K, Table S37 and Table A2 I Appendix 2†) and (ii) the fast components of the multi-exponential $Cr(^2E \rightarrow {}^4A_2)$ decay traces account for less than 20% of total intensities in the dinuclear complexes, we assume that the powder samples of $[Cl_3Cr(L)CrCl_3]$ (L = tppz, ebbt) and $[(tpy)Cr(L)Cr(tpy)](PF_6)_6$ complexes (L = bbt, ebbt) possess two non-equivalent chromium sites as found in the crystal structures of $[Cr_2Cl_6(tppz)]\cdot 3C_5H_9NO$ (**11**) and $[Cr_2(tpy)_2(bbt)](PF_6)_6\cdot 8CH_3CN\cdot(CH_3CH_2)_2O$ (**13**). The energies of the two $Cr(^2E)$ levels, referred to as D = donor and A = acceptor in the dinuclear complexes, are therefore slightly different and compatible with the operation of intramolecular intermetallic energy transfers characterized by their first-order rate constants $W_{D\rightarrow A}$ and $W_{A\rightarrow D}$ (Fig. 9a). This model was previously postulated by Castelli and Forster for rationalizing the multi-

Table 2 Experimental lifetimes found for the dinuclear $[Cl_3Cr(L)CrCl_3]$ and $[(tpy)Cr(L)Cr(tpy)](PF_6)_6$ complexes (L = tppz, bbt, ebbt) and intermetallic energy transfer rate constants $W_{D\rightarrow A}$ estimated with eqn (9)

Complex	T/K	τ_1/μs	τ_2/μs	$W_{D\rightarrow A}$/s^{-1}	Cr⋯Cr[a]/Å
$[Cr_2Cl_6(tppz)]$	5	3.6(1)	0.9(1)	$8(2)\times10^5$	6.660(2)
$[Cr_2Cl_6(bbt)]$	5	21(1)[b]	—	—	10.9261(8)
$[Cr_2Cl_6(ebbt)]$	3.5	3.6(1)	0.4(1)	$2.2(4)\times10^6$	—
$[Cr_2(tpy)_2(bbt)](CF_3SO_3)_6$	5	40.3(1)	2.3(1)	$4.1(8)\times10^5$	10.8957(5)
$[Cr_2(tpy)_2(ebbt)](PF_6)_6$	3.5	0.24(1)	0.04(1)	$2.1(4)\times10^7$	13.4669(6)

[a] Intermetallic distance measured in the crystal structures. [b] Mono-exponential decay.

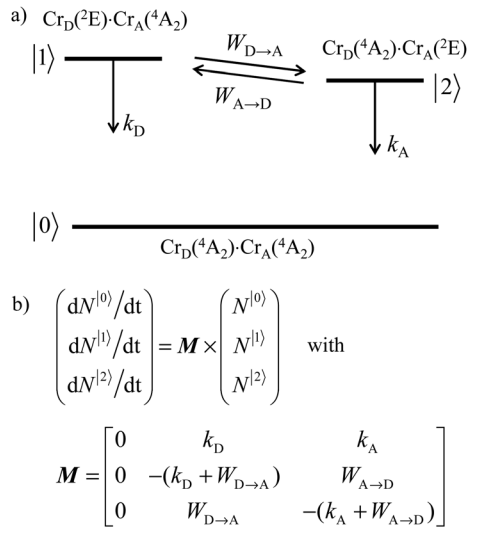

Fig. 9 (a) Energy level diagram and (b) kinetic matrix equations for the relaxation of the $Cr(^2E)$ excited levels occurring in a dinuclear chromium complex with non-equivalent metallic sites ($Cr_D\cdot Cr_A$). k_A and k_D are the first-order de-excitation rate constants (sum of radiative and non-radiative processes), whereas $W_{D\to A}$ and $W_{A\to D}$ are the intramolecular energy transfer rate constants.

exponential decay observed in solid samples of $[Cr(urea)_6]^{3+}$ chromophores.[124] It is further supported by the time-resolved luminescence spectra recorded for $[(tpy)Cr(bbt)Cr(tpy)]X_6$ (X = PF_6 in Fig. 7c and X = CF_3SO_3 in Fig. A2-13 in Appendix 2†), which show a faster decay of the high energy part of the emission band (corresponding to the lifetime of $Cr_D(^2E)$) followed by a longer decay for the low energy part (corresponding to the lifetime of $Cr_A(^2E)$).

Although the time evolution of the population densities of the three states ($N^{|i\rangle}$, i = 0, 1, 2) can be obtained by numerically solving the matrix kinetic equation shown in Fig. 9b with the help of projection operators and Lagrange–Sylvester formula,[125] reasonable approximations assume that (i) the back energy transfer is negligible ($W_{A\to D} \approx 0$) for time-resolved measurements performed below 5 K, (ii) the long-lived component τ_1 of the bi-exponential decay kinetic trace (Table 2, column 3) reflects the sum of radiative and non-radiative relaxation rate constants of the acceptor ($k_A \approx (\tau_1)^{-1}$ in Fig. 9) and (iii) τ_1 can also be taken as an acceptable estimation for the relaxation rate constant of the donor in the absence of acceptor ($k_D \approx k_A \approx (\tau_1)^{-1}$ in Fig. 9). With this in mind, the short-lived component τ_2 observed in the dinuclear complexes (Table 2, column 4) stands for the sum of the relaxation pathways affecting $Cr_D(^2E)$ (eqn (9) left), from which the intramolecular intermetallic energy transfer rate constants $W_{D\to A}$ can be easily deduced (eqn (9) and Table 2 column 5).

$$\frac{1}{\tau_2} = k_D + W_{D\to A} \Rightarrow W_{D\to A} = \frac{1}{\tau_2} - \frac{1}{\tau_1} \quad (9)$$

The first striking results concern the rather short characteristic lifetimes $0.2 \le \tau_1 \le 40$ μs measured for the $Cr(^2E)$ levels in the dinuclear complexes in the absence of energy transfer ($\tau_1 = (k_A)^{-1} \approx (k_D)^{-1}$, Table 2, column 3). The reduction by one to two orders of magnitude compared with related data recorded for the mononuclear analogues under the same experimental conditions (solid state, cryogenic temperatures, Table S37†) are reminiscent of the well-documented[4,127] effect of the reduction in ligand-field strength on the relaxation pathways affecting the $Cr(^2E)$ level. For a given chromophore (CrN_3Cl_3 in $[Cl_3Cr(L)CrCl_3]$ or CrN_6 in $[(tpy)Cr(L)Cr(tpy)](PF_6)_6$), we additionally detect a surprising counter-intuitive increase of the intermetallic energy transfer rate constant for larger intramolecular Cr···Cr distances (Table 2). According to the Fermi's golden rule summarized in eqn (10), the rate of resonant intermetallic energy transfer depends on (i) the spectral overlap integral Ω_{DA} between the absorption spectrum of the acceptor A, and the emission spectrum of the donor D and (ii) the perturbation operator H_p usually modelling the magnitude of through-space (multipolar electrostatic) and/or through-bond (double electronic exchange) communication.[75,126]

$$W_{D\to A} \propto (2\pi/\hbar)|\langle DA^*|H_p|D^*A\rangle|^2\Omega_{DA} \quad (10)$$

Since the energies of the narrow and weakly Stokes-shifted spin–flip $Cr(^2E \leftrightarrow {}^4A_2)$ transitions do not significantly depend on the ligand-field strength, the 810–1080 cm^{-1} spectral widths measured for the $Cr(^2E \to {}^4A_2)$ phosphorescence band in the dinuclear complexes (Fig. A2-4 to A2-8 in Appendix 2†) are compatible with non-negligible and comparable spectral overlap integrals Ω_{DA} along the complete series. We therefore assign the unusually large energy transfer rate constants operating in the longest rod-like dyads $[Cl_3Cr(ebbt)CrCl_3]$ ($W_{D\to A} = 2.2(4) \times 10^6$ s^{-1}) and $[(tpy)Cr(ebbt)Cr(tpy)]^{6+}$ ($W_{D\to A} = 2.1(4) \times 10^7$ s^{-1}) to the exceptional through-bond conducting character of alkyne-containing bridges doped with aromatic rings,[121,122] a trend in line with magnetic data (see the previous section). For unsolvated crystals of $[Cr_2Cl_6(bbt)]$ (**12**), the center of symmetry found in the crystal structure is maintained in the powder sample and a mono-exponential decay is observed (Table 2, entry 2), in agreement with the kinetic model for which $k_A = k_D$ and $W_{D\to A} = W_{A\to D}$.[128]

Unravelling intermetallic communication in dinuclear $[Cl_3Cr(L)CrCl_3]$, $[(tpy)Cr(L)Cr(tpy)](PF_6)_6$ complexes (L = tppz, bbt, ebbt): thermodynamic evidence

The failure to isolate the dinuclear $[(tpy)Cr(tppz)Cr(tpy)](PF_6)_6$ complex from the reaction of $[(tpy)Cr(CF_3SO_3)_3]$ with tppz (Fig. 5) suggests the operation of a strong anti-cooperative protocol for the successive binding of two $[Cr(tpy)]^{3+}$ to the bridging tppz ligand. The spectrophotometric titrations of $[(tpy)Cr(tppz)]^{3+}$ with Er^{3+} in acetonitrile (Er^{3+} stands for a labile and non-hydrolyzable substitute of $[Cr(tpy)]^{3+}$) confirms the lack of affinity of the available tridentate site of tppz in $[(tpy)Cr(tppz)]^{3+}$ for a second trivalent cation ($\beta_{11}^{Cr(tppz),Er} \ll 50$ in equilibrium (11), Fig. 10).[129] A quantitative assessment of the

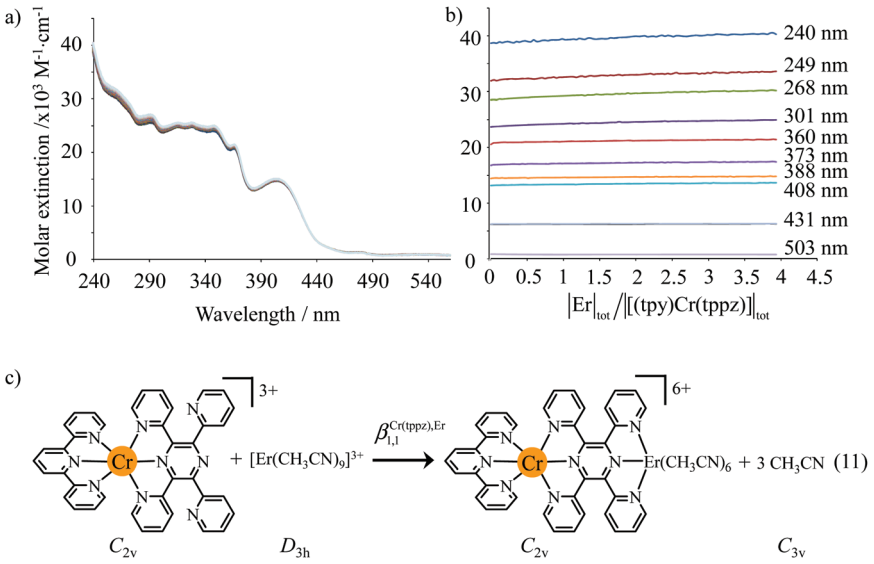

Fig. 10 (a) Variation of absorption spectra, (b) corresponding variation of molar extinctions and (c) proposed modeling ($\beta_{1,1}^{Cr(tppz),Er} \ll 50$) for the titration of $[(tpy)Cr(tppz)]^{3+}$ (2×10^{-4} M) with $Er(CF_3SO_3)_3$ in acetonitrile (298 K).

searched cooperative factors can be approached by the spectrophotometric titrations of the bridging ligand tppz (or bbt) with $Er(CF_3SO_3)_3$ in acetonitrile : chloroform = 65 : 35 (Fig. 11). The resulting changes in the absorption spectra are characterized by smooth end points occurring at Eu : L = 1 : 3, Eu : L = 1 : 2, Eu : L = 1 : 3 and Eu : L = 1 : 1 (Fig. 11a and b for L = tppz and Fig. S24a for L = bbt in the ESI†). Factor analysis (Fig. 11c and Fig. S24c†)[130] followed by non-linear least square fits[131] to equilibria (12)–(15) (Fig. 11e) provide satisfying re-constructed individual absorption spectra (Fig. 11d and Fig. S24d†) together with macroscopic formation constants gathered in Table 3 (entries 1–4).

Monitoring these titrations using light-scattering techniques did not reveal any sign of aggregation due to the formation of two-dimensional and three-dimensional polymers as postulated by Long and coworkers for related reactions involving a back-to-back bis-terdentate ligand and $Eu(NO_3)_3$.[132] Application of the site binding model (eqn (16))[133] to equilibria (12)–(15) leads to eqn (17)–(20), which model the complete complexation process with only four parameters. (1) $\omega_{m,n}^{Er,L}$ stands for pure entropic contribution to the complexation reaction brought by the change in the rotational entropy when the reactants are transformed into products (Appendix 3 in the ESI†).[134] (2) $f_{N_3,L}^{Er}$ represents the intrinsic affinity of Er^{3+} for the tridentate binding unit of the bridging ligand (including desolvation processes). (3) $u_{Er}^{L,L} = \exp(-\Delta E_{Er}^{L,L}/RT)$, respectively (4) $u_{L}^{Er,Er} = \exp(-\Delta E_{L}^{Er,Er}/RT)$ are the cooperative effects, in terms of Boltzmann factors, which accompany the successive binding of ligands to the same metallic centre ($u_{Er}^{L,L}$), respectively, the successive binding of metals to the same bridging ligand ($u_{L}^{Er,Er}$). Multi-linear least-square fits of eqn (17)–(20) to the experimental stability constants provided the thermodynamic descriptors collected in Table 3 (entries 5–7).

$$\beta_{m,n}^{Er,L} = \omega_{m,n}^{Ln,L} \cdot \prod f_{N_3,L}^{Er} \cdot \prod u_{Er}^{L,L} \cdot \prod u_{L}^{Er,Er} \quad (16)$$

$$\beta_{1,1}^{Er,L} = \omega_{1,1}^{Er,L} f_{N_3,L}^{Er} = 12 f_{N_3,L}^{Er} \quad (17)$$

$$\beta_{1,2}^{Er,L} = \omega_{1,2}^{Er,L} (f_{N_3,L}^{Er})^2 u_{Er}^{L,L} = 48 (f_{N_3,L}^{Er})^2 u_{Er}^{L,L} \quad (18)$$

$$\beta_{1,3}^{Er,L} = \omega_{1,3}^{Er,L} (f_{N_3,L}^{Er})^3 (u_{Er}^{L,L})^3 = 128 (f_{N_3,L}^{Er})^3 (u_{Er}^{L,L})^3 \quad (19)$$

$$\beta_{2,1}^{Er,L} = \omega_{2,1}^{Er,L} (f_{N_3,L}^{Er})^2 u_{L}^{Er,Er} = 72 (f_{N_3,L}^{Er})^2 u_{L}^{Er,Er} \quad (20)$$

The intrinsic affinity of the tridentate N_3 binding units for the entering trivalent Er^{3+} cation in the bridging bbt ligand $\Delta G_{N_3,bbt}^{Er} = -2.303 \cdot RT \log(f_{N_3,bbt}^{Er}) = -40(2)$ kJ mol^{-1} perfectly matches the one previously reported for the monomeric precursor terpyridine (tpy) ligand under similar conditions (acetonitrile, 298 K).[135] This implies that, beyond an obvious statistical factor of 2, the connection of a second tridentate binding unit in the back of the original terpyridine units to give bbt has little effect on the binding properties of the tridentate N_3 site taken separately. As expected, the successive binding of several tridentate N_3 units to the same trivalent Er^{3+} centre is accompanied by some minor anti-cooperative processes ($\Delta E_{Er}^{L,L}$ = 9(2) kJ mol^{-1} for bbt and 6(2) kJ mol^{-1} for tpy) resulting from the stepwise neutralization of the positive metallic charge by an increasing number of bound nitrogen donors.[135] With this in mind, it appears logical that the much less basic bridging pyrazine ring found in tppz (pK_a = 0.37),[136] compared with the 4,4′-bipyridine bridge in bbt (pK_a = 4.8),[137] leads to both a reduced affinity for Er^{3+} ($\Delta G_{N_3,tppz}^{Er} = -32(2)$ kJ mol^{-1}) and a smaller ligand–ligand interaction ($\Delta E_{Er}^{tppz,tppz}$ = 5(3)

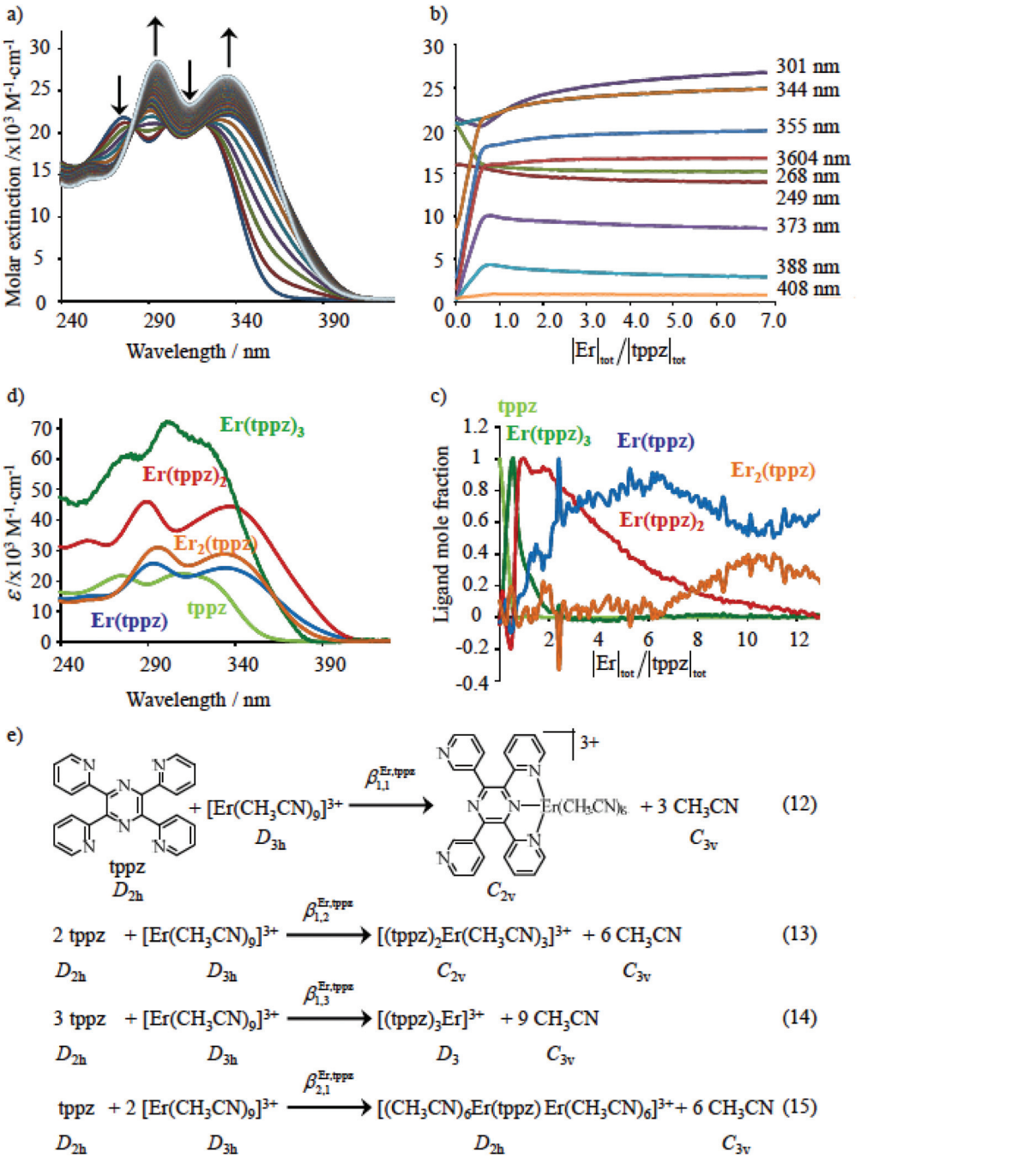

Fig. 11 (a) Variation of absorption spectra and (b) corresponding variation of observed molar extinctions at different wavelengths observed for the spectrophotometric titration of tppz with $Er(CF_3SO_3)_3$ (total ligand concentration: 8×10^{-5} mol dm^{-3} in $CH_3CN : CHCl_3 = 65 : 35$, 298 K). (c) Evolving factor analysis using five absorbing eigenvectors,[130] (d) re-constructed individual electronic absorption spectra[131] and (e) proposed thermodynamic model.

kJ mol^{-1}). However, the most noteworthy thermodynamic result concerns the considerable anti-cooperative mechanism accompanying the successive fixation of two Er^{3+} cations onto the bridging ligand, which are diagnostic for the operation of intermetallic electrostatic communication on the nanometric scale in these polyaromatic dyads. The large value $\Delta E^{Er,Er}_{tppz}$ = 18(5) kJ mol^{-1} found for the short-bridging tppz ligand combined with its limited intrinsic affinity $\Delta G^{Er}_{N_3,tppz}$ explains the difficulties in isolating dinuclear $[X_3Cr(tppz)CrX_3]$ complexes. The smaller anti-cooperative effect observed for bbt ($\Delta E^{Er,Er}_{bbt}$ = 12(5) kJ mol^{-1}) restores sufficient affinity for the formation of dinuclear $[X_3Cr(bbt)CrX_3]$ complexes.

Table 3 Experimental stability constants ($\log(\beta^{Er,L}_{m,n})$) and microscopic thermodynamic parameters fitted with eqn (17)–(20) for the reaction of tppz or bbt with $Er(CF_3SO_3)_3$ in acetonitrile/chloroform (65 : 35) at 298 K

Ligand	tppz	bbt
$\log(\beta^{Er,L}_{1,1})$	6.42(2)	8.19(16)
$\log(\beta^{Er,L}_{1,2})$	12.03(3)	13.76(32)
$\log(\beta^{Er,L}_{1,3})$	15.89(4)	18.16(50)
$\log(\beta^{Er,L}_{2,1})$	9.80(3)	13.63(16)
$\log(f^{Er}_{N_3,L})/\Delta G^{Er}_{N_3,L}$ in kJ mol^{-1} [a]	5.5(4)/−32(2)	6.9(4)/−40(2)
$\log(^{L,L}_{Er})/\Delta E^{L,L}_{Er}$ in kJ mol^{-1} [b]	−0.9(5)/5(3)	−1.6(5)/9(2)
$\log(u^{Er,Er}_{L})/\Delta E^{Er,Er}_{L}$ in kJ mol^{-1} [c]	−3.1(9)/18(5)	−2.1(9)/12(5)
AF[d]	1.23×10^{-2}	9.46×10^{-3}

[a] $\Delta G^{Er}_{N_3,L} = -2.303RT\log(f^{Er}_{N_3,L})$. [b] $\Delta E^{L,L}_{Er} = -2.303RT\log(u^{L,L}_{Er})$. [c] $\Delta E^{Er,Er}_{L} = -2.303{\cdot}RT\log(u^{Er,Er}_{L})$. [d] Agreement factor $AF = \sqrt{\sum_{m,n}(\log(\beta^{Er,L}_{m,n,exp}) - \log(\beta^{Er,L}_{m,n,calcd}))^2 / \sum_{m,n}(\log(\beta^{Er,L}_{m,n,exp}))^2}$.

Conclusion

The synthetic method developed by Housecroft and Constable[46] for the preparation of a semi-labile [(tpy)$Cr(O_3SCF_3)_3$] precursor can be successfully applied for [(tppz)$Cr(O_3SCF_3)_3$], but failed for the slightly more basic bis-benzimidazole derivative ebzpy, which is decomplexed from Cr^{III} in trifluoromethanesulfonic acid. A subsequent reaction of [(L)$Cr(O_3SCF_3)_3$] (L = tpy, tppz) with a second tridentate binding unit L′ leads to the targeted heteroleptic mononuclear $[(L)Cr(L')]^{3+}$ complexes, a procedure which can be extended for the preparation of unprecedented dinuclear rod-like $[(tpy)Cr(L')Cr(tpy)]^{6+}$ dyads when [(tpy)$Cr(O_3SCF_3)_3$] is reacted with the Janus-type bis-terdentate receptors L′ = bbt or ebbt. In other words, [(tpy)$Cr(O_3SCF_3)_3$] can be considered as an analogue of $[(tpy)Ru(DMSO)Cl_2]$[138] for the introduction of $[(tpy)M]^{z+}$ fragments into (supra)molecular architectures, thus opening large avenues for the selective introduction of trivalent $[CrN_6]^{3+}$ chromophores in linear dyads and triads, and in di- and tridimensional networks similar to those designed with Ru^{II}.[19–24] While the assessment of the degree of communication between Ru^{II} centres requires partial reduction to get mixed-valence systems, the paramagnetic and spin-only character of Cr^{III} centres offers a straightforward access to this parameter with the simple determination of the isotropic magnetic coupling constants. For the $[Cl_3Cr(L)CrCl_3]$ and $[(tpy)Cr(L)Cr(tpy)]^{6+}$ dyads investigated here as proof-of-concept, the distance dependence of the magnetic communication reveals subtle modulations due to ligand-field effects and orbital overlap, which are optimized when two CrN_6 chromophores are connected through an alkyne bridge in $[(tpy)Cr(ebbt)Cr(tpy)]^{6+}$. Again, compared with Ru^{II} (strong-field low-spin d^6 electronic configuration), the photophysical properties of Cr^{III} (d^3 electronic configuration) are better suited for unravelling intermetallic communication *via* the straightforward determination of ligand-field and Racah parameters, which are difficult to address in analogous ruthenium complexes. Moreover, minor non-equivalence of the Cr^{III} coordination sites is accompanied by efficient intramolecular intermetallic energy transfer processes, the rate constants of which can be exploited for estimating the efficiency of intermetallic interactions. Finally, our fear that the successive connection of two triply-charged Cr^{III}-type cations (instead of two divalent Ru^{II}-type cations) to a Janus-type bridging ligand may be hindered by a strong (electrostatic) anti-cooperative contribution seems only justified for the smallest pyrazine bridge in tppz. For the longer distance found in bbt, the anti-cooperative factor estimated with Er^{3+} taken as a trivalent model cation is reduced to such an extent that successive metallic complexation processes become accessible as demonstrated by the isolation of $[Cr_2(tpy)_2(bbt)](PF_6)_6$ and $[Cr_2(tpy)_2(ebbt)](PF_6)_6$ in fair to good yields.

Experimental section

Solvents and starting materials

2,2′:6′,2″-Terpyridine (tpy) and the Janus-type bridging ligand tetra-2-pyridinylpyrazine (tppz) are commercially available. 2,6-Bis(1-ethyl-1*H*-benzo[*d*]imidazol-2-yl) pyridine (ebzpy),[90] *N*,*N*′-dimethyl-*N*,*N*″-dipyridin-2-ylpyridine-2,6-diamine (ddpd)[120] and 6′,6″-di(pyridin-2-yl)-2,2′:4′,4″:2″,2‴-quaterpyridine (bbt)[139] were synthesized according to the published procedures. The synthesis of 4′,4‴-(ethynyl)bis(2,2′:6′,2″-terpyridine) (ebbt) was adapted from the literature (Appendix 4†).[109] Reagent grade acetonitrile (ACN) and chloroform were distilled from CaH_2 when needed. All other chemicals were purchased from commercial suppliers and used without further purification. Silica-gel plates (Merck, 60 F_{254}) were used for thin-layer chromatography. Preparative column chromatography was performed using either neutral alumina gel from Fluka (Typ 507 C) 100–125 mesh or SiliaFlash® silica gel P60 (0.04–0.063 mm).

Synthesis of gallium and chromium complexes

All complexes were characterized by IR spectroscopy (Tables S41–S44†) and gave satisfying elemental analyses (Table S1†).

$[Ga(tpy)_2](PF_6)_3$. A solution of $Ga(CF_3SO_3)_3$ (60.5 mg, 0.117 mmol, 1 eq.) in degassed acetonitrile was added into a solution of terpyridine (54.8 mg, 0.235 mmol, 2.01 eq.) in distilled acetonitrile (20 mL). The color of the mixture immediately turned yellow. After being stirred at 50 °C overnight, acetonitrile was evaporated and the resulting solid was re-solubilized in methanol (5–8 mL). A solution of saturated $(n\text{-}Bu)_4NPF_6$ (2.5 mL, C = 90–100 mg mL^{-1}) was added and the resulting pale yellow precipitate was filtered, washed with dichloromethane (2 × 5 mL) and diethyl ether (2 × 5 mL) and dried under vacuum to obtain $[Ga(tpy)_2](PF_6)_3$ as a yellow powder (98 mg, 0.101 mmol, yield 86%). Slow diffusion of diethyl ether into a solution of the complex in acetonitrile gave pale yellow single crystals of $[Ga(tpy)_2](PF_6)_3{\cdot}2CH_3CN$ (**1**) suitable for X-ray diffraction studies. ^{1}H NMR of $[Ga(tpy)_2](PF_6)_3$ (CD_3CN, 400 MHz, δ/ppm): 9.10 (6H, m), 8.80 (4H, d, ^3J = 8 Hz), 8.43 (4H, td, ^3J = 8 Hz, ^4J = 0.8 Hz), 7.74 (4H, d, ^3J = 8 Hz),

7.63 (4H, t, ^3J = 8 Hz). ESI-MS (CH_3CN) m/z: 825.8 ($[Ga(tpy)_2(PF_6)_2]^+$), 339.8 ($[Ga(tpy)_2(PF_6)]^{2+}$) and 178.7 ($[Ga(tpy)_2]^{3+}$).

$[Cr(tpy)_2](PF_6)_3$. In a glovebox, a solution of $Cr(CF_3SO_3)_2{\cdot}H_2O$ (166 mg, 0.450 mmol, 1 eq.)[48] in degassed acetonitrile was added into a solution of terpyridine (209 mg, 0.895 mmol, 1.99 eq.) in degassed acetonitrile (20 mL). The color of the mixture immediately turned deep dark green. After being stirred at 45 °C for 4 hours, a solution of $(n\text{-}Bu)_4NCF_3SO_3$ (177 mg, 0.450 mmol, 1 eq.) in degassed acetonitrile (2 mL) was added. The Schlenk tube was transferred into the lab and Cr(II) was oxidized by bubbling dioxygen. The colour changed to red-orange. After being stirred for 1 hour at RT, acetonitrile was evaporated and the resulting solid was solubilized in hot methanol (20 mL). A solution of saturated $(n\text{-}Bu)_4NPF_6$ in methanol (4 mL, C = 100 mg ml^{-1}) was added into the solution in order to precipitate a red-orange complex, which was filtered, washed with dichloromethane (3 × 15 mL) and diethyl ether (3 × 10 mL) and dried under vacuum to obtain a red-orange powder $[Cr(tpy)_2](PF_6)_3$ (326 mg, 0.342 mmol, yield 76%). Slow diffusion of diethyl ether into a solution of the complex in acetonitrile gave red-orange single crystals of $[Cr(tpy)_2](PF_6)_3{\cdot}2.5CH_3CN$ (**2**) suitable for X-ray diffraction studies.

$[Cr(ebzpy)_2](PF_6)_3$. In a glovebox, a sky blue solution of $Cr(CF_3SO_3)_2{\cdot}H_2O$ (155 mg, 0.420 mmol, 1 eq.)[48] in degassed acetonitrile was introduced into a 50 mL Schlenk tube containing a solution of 2,6-bis(1-ethyl-1*H*-benzo[*d*]imidazol-2-yl)pyridine (ebzpy, 307 mg, 0.835 mmol, 1.99 eq.) in degassed acetonitrile (20 mL). The blue color of the Cr(II) solution turned immediately dark green. After being stirred at 45 °C for 4 hours, a solution of $(n\text{-}Bu)_4NCF_3SO_3$ (165 mg, 0.420 mmol, 1 eq.) in degassed acetonitrile (2 mL) was added. The Schlenk tube was transferred into the lab and the Cr(II) was oxidized by bubbling dioxygen. The colour of the solution changed to red-orange to give $[Cr(ebzpy)_2](CF_3SO_3)_3$. The red-orange acetonitrile solution of $[Cr(ebzpy)_2](CF_3SO_3)_3$ was evaporated and the resulting solid was solubilized in hot methanol (20 mL). Anion metathesis was performed by adding 4 mL of a saturated solution of $(n\text{-}Bu)_4NPF_6$ in methanol (100 mg mL^{-1}). The red-orange precipitate was filtered, washed with dichloromethane (3 × 15 mL) and diethyl ether (3 × 10 mL) and dried under vacuum to give $[Cr(ebzpy)_2](PF_6)_3$ as a red-orange powder (385 mg, 0.315 mmol, yield 75%). Slow diffusion of diethyl ether into a solution of the complex in acetonitrile gave red-orange single crystals of $[Cr(ebzpy)_2](PF_6)_3{\cdot}5.5CH_3CN$ (**3**) suitable for X-ray diffraction studies. Slow diffusion of diethyl ether into a solution of the intermediate $[Cr(ebzpy)_2](CF_3SO_3)_3$ complex in acetonitrile gave red-orange single crystals of $[Cr(ebzpy)_2](CF_3SO_3)_3{\cdot}2CH_3CN$ (**4**) suitable for X-ray diffraction studies as well.

$[Cr(ebzpy)Cl_3]$. A solution of 2,6-bis(1-ethyl-1*H*-benzo[*d*]imidazol-2-yl)pyridine (182 mg, 0.495 mmol, 1.01 eq.) in dry dichloromethane (5 mL) was dropwise added into a solution of $[CrCl_3(THF)_3]$ (184 mg, 0.490 mmol, 1 eq.) in dry dichloromethane (30 mL). The color of the mixture changed from purple to green. After being stirred at room temperature for 24 hours, the mixture was filtered and the solid was washed with dichloromethane (3 × 15 mL) and diethyl ether (3 × 10 mL), and dried under vacuum to give $[Cr(ebzpy)]Cl_3$ (253 mg, 0.47 mmol, yield 98%). Slow diffusion of diethyl ether into a solution of a complex in DMF gave dark green single crystals of $[Cr(ebzpy)Cl_3]{\cdot}DMF$ (**5**) suitable for X-ray diffraction studies. The complex was characterized by elemental analysis (Table S1†).

$[Cr(tppz)Cl_3]$. Tetra-2-pyridinylpyrazine (tppz) (170 mg, 0.438 mmol, 2 eq.) was suspended in a distilled mixture of acetonitrile and ethanol (25 mL : 25 mL) and heated under reflux. A solution of $[CrCl_3(THF)_3]$ in acetonitrile (82 mg, 0.219 mmol, 1 eq.) was added dropwise to the tppz solution mixture, the colour of which immediately turned from purple to green. After being stirred and refluxed for 24 hours under an inert N_2 atmosphere, the insoluble product was filtered (micro-filtering), then washed with a hot solution of acetonitrile and ethanol (1 : 1) for removing the excess ligand. The resulting solid was washed with diethyl ether (3 × 7 mL) and dried under vacuum to give $Cr(tppz)Cl_3$ (114 mg, 0.208 mmol, yield 95%). Slow diffusion of diethyl ether into a solution of the complex in DMF gave dark green single crystals of $[Cr(tppz)Cl_3]{\cdot}2DMF$ (**6**) suitable for X-ray diffraction studies.

$Cr(tppz)(SO_3CF_3)_3$. $Cr(tppz)Cl_3$ (140 mg, 0.256 mmol, 1 eq.) and triflic acid (300 μL, 3.4 mmol, 13 eq.) were loaded into a 50 mL Schlenk tube under a N_2 atmosphere. The green colour of the complex turned to dark red immediately together with gas escape of HCl (confirmed by precipitation of AgCl when bubbling into an aqueous solution of $AgNO_3$). After being stirred at room temperature for 3 hours, the dark red complex of $Cr(tppz)(CF_3SO_3)_3$ was precipitated by the addition of 25 mL of diethyl ether. The complex was filtered, washed with diethyl ether (3 × 6 mL) and dried under vacuum to give $Cr(tppz)(CF_3SO_3)_3$ (204 mg, 0.230 mmol, yield 90%).

$[Cr(ebzpy)(tpy)](PF_6)_3$. A dark red solution of $[Cr(tpy)(CF_3SO_3)_3]$ (168 mg, 0.230 mmol, 1 eq.) in distilled acetonitrile was loaded into a 50 mL Schlenk tube under an inert N_2 atmosphere. A solution of 2,6-bis(1-ethyl-1*H*-benzo[*d*]imidazol-2-yl) pyridine (85 mg, 0.230 mmol, 1 eq.) in acetonitrile (8–10 mL) was added to the Schlenk tube. The mixture was refluxed under N_2 for 3 hours, then the solution was evaporated to dryness and the residual solid solubilized in distilled acetonitrile (3 mL). Slow diffusion of diethyl ether into the concentrated solution of the complex in acetonitrile gave $[Cr(tpy)(ebzpy)](CF_3SO_3)_3$ as red crystals (126 mg, 0.115 mmol, yield 50%). $[Cr(tpy)(ebzpy)](CF_3SO_3)_3$ was solubilized in MeOH, then anion metathesis was initiated by adding 4 mL of a saturated solution of tetrabutylammonium hexafluorophosphate [$(n\text{-}Bu)_4NPF_6$] in methanol (100 mg mL^{-1}). The resulting red-orange precipitate was filtered, washed with diethyl ether and dried under vacuum to give $[Cr(tpy)(ebzpy)](PF_6)_3$. Slow diffusion of diethyl ether in a concentrated solution of the complex in acetonitrile (3 ml) produced red single crystals of $[Cr(tpy)(ebzpy)](PF_6)_3{\cdot}2CH_3CN$ (**7**) suitable for X-ray diffraction studies.

$[Cr(tppz)(tpy)](PF_6)_3$. A solution of $Cr(tppz)(CF_3SO_3)_3$ (177.5 mg, 0.2 mmol, 1 eq.) in distilled acetonitrile was drop-

wise added into a concentrated solution of terpyridine in acetonitrile (58 mg, 0.25 mmol in 8 mL). The solution became warm during the addition and was then refluxed for 3 hours. The resulting mixture was cooled, filtered and the remaining dark-red solution was evaporated to dryness. Slow diffusion of diethyl ether into a concentrated solution of the complex in acetonitrile (3 ml) produced yellow single crystals of [Cr(tppz)(tpy)]$(CF_3SO_3)_3$ suitable for X-ray diffraction studies in approximately 40–50% yields. [Cr(tppz)(tpy)]$(CF_3SO_3)_3$ was solubilized in MeOH, then anion metathesis was initiated by adding 4 mL of a saturated solution of tetrabutylammonium hexafluorophosphate [$(n\text{-Bu})_4NPF_6$] in methanol (100 mg mL^{-1}). The resulting red-orange precipitate was filtered, washed with diethyl ether and dried under vacuum to give [Cr(tppz)(tpy)]$(PF_6)_3$ (104 mg, 0.094 mmol, yield 47%). Slow diffusion of diethyl ether in a concentrated solution of the complex in acetonitrile (3 ml) produced red single crystals of [Cr(tpy)(tppz)]$(PF_6)_3\cdot 3CH_3CN$ (**8**) suitable for X-ray diffraction studies.

[Cr_2Cl_6(tppz)]. Tetra-2-pyridinylpyrazine (220 mg, 0.566 mmol, 1 eq.), $CrCl_3$, $6H_2O$ (440 mg, 1.65 mmol, 2.9 eq.), and EtOH (12 mL) were introduced into a round bottom flask. After complete dissolution of $CrCl_3$, acetonitrile (24 mL) was added to the resulting green solution, and the mixture was refluxed for 24 hours. The brown greenish precipitate was filtered off, washed with boiling EtOH (4 times), and dried with diethylether to give [Cr_2Cl_6(tppz)] as a brown greenish solid (390 mg, 0.555 mmol, yield 98%). Slow diffusion of diethylether in a concentrated solution of the [Cr_2Cl_6(tppz)] complex in *N*-methyl-2-pyrrolidone (NMP) provided green crystals of [Cr_2Cl_6(tppz)]$\cdot 3C_5H_9NO$ (**11**) suitable for X-ray diffraction studies.

[Cr_2Cl_6(bbt)]. 6′,6″-Bis(2-pyridyl)-2,2′:4′,4:2″,2‴-quaterpyridine (bbt, 50 mg, 0.108 mmol, 1 eq.), $CrCl_3$, $6H_2O$ (86 mg, 0.323 mmol, 3 eq.), and DMF (10 mL) were introduced into a round bottom flask. The mixture was stirred at 90 °C for 64 hours. The green precipitate was filtered on a PTFE membrane, washed with EtOH, and dried with diethylether to give $Cr_2Cl_6(bbt)\cdot H_2O$ (83 mg, 0.089 mmol, yield 96%) as a green solid. Slow diffusion of diethylether in a saturated solution of the [Cr_2Cl_6(bbt)] complex in *N*-methyl-2-pyrrolidone (NMP) provided green crystals of [Cr_2Cl_6(bbt)] (**12**) suitable for X-ray diffraction studies.

[Cr_2Cl_6(ebbt)]. 4′,4⁗-(Ethynyl)bis(2,2′:6′,2″-terpyridine) (ebbt, 74 mg, 0.151 mmol, 1 eq.), $CrCl_3$, $6H_2O$ (121 mg, 0.454 mmol, 3 eq.), and DMF (20 mL) were introduced into a round bottom flask. The mixture was stirred at 90 °C for 64 hours. The green precipitate was filtered on a PTFE membrane, washed with EtOH, and dried with diethylether to give [Cr_2Cl_6(ebbt)]$\cdot 2H_2O$ as a green solid (34 mg, 0.041 mmol, yield 27%). Due to the very low solubility of this complex in common organic solvents, we were not able to obtain crystals suitable for X-ray diffraction studies.

[Cr_2(tpy)$_2$(bbt)]$(PF_6)_6$. 6′,6″-Bis(2-pyridyl)-2,2′:4′,4:2″,2‴-quaterpyridine (bbt) (30 mg, 0.065 mmol, 1 eq.), and distillated $CHCl_3$ (12 mL) were introduced into a Schlenk tube under argon. After complete ligand dissolution, a solution of [Cr(tpy)$(SO_3CF_3)_3$] (109 mg, 0.148 mmol, 2.3 eq.)[46] dissolved in distilled acetonitrile (4 mL) was added. The mixture was stirred at 70 °C for 15 hours. The orange precipitate was filtered, washed with dichloromethane, and dried with diethylether. The orange solid so obtained was recrystallized from EtOH and dried with diethylether to give [Cr_2(tpy)$_2$(bbt)]$(SO_3CF_3)_3$ (92 mg, 0.048 mmol, yield 74%) as an orange solid. [Cr_2(tpy)$_2$(bbt)]$(SO_3CF_3)_3$ was dissolved in MeOH, and a saturated solution of $TBAPF_6$ in MeOH was slowly added until complete precipitation of the yellow compound. The precipitate was filtered, washed with a few drops of MeOH, and dried with diethylether, to provide [Cr_2(tpy)$_2$(bbt)]$(PF_6)_6$ as a yellow solid. Slow diffusion of diethylether into a solution of [Cr_2(tpy)$_2$(bbt)]$(PF_6)_6$ in acetonitrile provided orange crystals of [Cr_2(tpy)$_2$(bbt)]$(PF_6)_6\cdot 8CH_3CN\cdot(CH_3CH_2)_2O$ (**13**) suitable for X-ray diffraction studies. ESI-MS *m*/*z*: [Cr_2(tpy)$_2$(bbt); $5SO_3CF_3]^+$ calc: 1779.0, found: 1780.3; [Cr_2(tpy)$_2$(bbt); $4SO_3CF_3]^{2+}$ calc: 815.0, found: 814.3; [Cr_2(tpy)$_2$(bbt); $3SO_3CF_3]^{3+}$ calc: 493.7, found: 493.6.

[Cr_2(tpy)$_2$(ebbt)]$(PF_6)_6$. 4′,4⁗-(Ethynyl)bis(2,2′:6′,2″-terpyridine) (ebbt, 40 mg, 0.082 mmol, 1 eq.), and distillated $CHCl_3$ (15 mL) were introduced into a Schlenk tube under argon. After complete ligand dissolution, a solution of [Cr(tpy)$(SO_3CF_3)_3$] (180 mg, 0.246 mmol, 3 eq.) dissolved in distilled acetonitrile (5 mL) was added. The mixture was stirred at 70 °C for 15 hours. The orange precipitate was filtered, washed with dichloromethane and dried with diethylether. The resulting orange solid was recrystallized from EtOH and dried with diethylether to give [Cr_2(tpy)$_2$(ebbt)]$(SO_3CF_3)_6$ (130 mg, 0.066 mmol, yield 81%) as an orange solid. [Cr_2(tpy)$_2$(ebbt)]$(SO_3CF_3)_6$ was dissolved in MeOH, and a saturated solution of $TBAPF_6$ in MeOH was slowly added until complete precipitation of the yellow compound. The precipitate was filtered, washed with a few drops of MeOH, and dried with diethylether to give [Cr_2(tpy)$_2$(ebbt)]$(PF_6)_6$ as a yellow solid. Slow diffusion of diethylether into a solution of the [Cr_2(tpy)$_2$(ebbt)]$(PF_6)_6$ complex in acetonitrile provided orange crystals of [Cr_2(tpy)$_2$(ebbt)]$(PF_6)_6\cdot 10CH_3CN$ (**14**) suitable for X-ray diffraction studies. ESI-MS *m*/*z*: [Cr_2(tpy)$_2$(ebbt); $5SO_3CF_3]^+$ calc: 1803.0, found: 1803.4; [Cr_2(tpy)$_2$(ebbt); $4SO_3CF_3]^{2+}$ calc: 827.0, found: 827.8; [Cr_2(tpy)$_2$(ebbt); $3SO_3CF_3]^{3+}$ calc: 501.7, found: 502.3; [Cr_2(tpy)$_2$(ebbt); $2SO_3CF_3]^{4+}$ calc: 339.0, found: 339.7; [Cr_2(tpy)$_2$(ebbt); $1SO_3CF_3]^{5+}$ calc: 241.4, found: 241.8; [Cr_2(tpy)$_2$(ebbt)]$^{6+}$ calc: 176.4, found: 176.9.

[$CrCl_3$(ddpd)]. *N*,*N*′-Dimethyl-*N*,*N*′-dipyridin-2-ylpyridine-2,6-diamine (ddpd) (80 mg, 0.274 mmol, 1 eq.), $CrCl_3$, $6H_2O$ (95 mg, 0.357 mmol, 1.3 eq.), and EtOH (20 mL) were introduced into a round bottom flask. After refluxing for 15 hours, a green precipitate formed was filtered and dried with diethylether to give [$CrCl_3$(ddpd)] (75 mg, 0.167 mmol, yield 61%) as a green solid. Slow diffusion of diethylether into a concentrated solution of [$CrCl_3$(ddpd)] in DMF provided green crystals of [$CrCl_3$(ddpd)] (**15**) suitable for X-ray diffraction studies.

Spectroscopic and analytical measurements

^1H and ^{13}C NMR spectra were recorded on a Bruker Avance 400 MHz spectrometer equipped with a variable temperature

unit. Chemical shifts are given in ppm with respect to tetramethylsilane $Si(CH_3)_4$. Pneumatically-assisted electrospray (ESI) mass spectra were recorded from 10^{-4} M solutions on an Applied Biosystems API 150EX LC/MS System equipped with a Turbo Ionspray source®. Elemental analyses were performed by K. L. Buchwalder from the Microchemical Laboratory of the University of Geneva. Spectrophotometric titrations were performed with a J&M diode array spectrometer (Tidas series) connected to an external computer. In a typical experiment, 50 cm^3 of ligand in acetonitrile : chloroform (65 : 35) (8×10^{-5} mol dm^{-3}) were titrated at 298 K with a solution of $Er(CF_3SO_3)_3$ (2×10^{-3} mol dm^{-3}) in the same solvent under an inert atmosphere. After each addition of 0.10 mL, the absorbance was recorded using a Hellma optrode (optical path length 0.1 cm) immersed in the thermostated titration vessel and connected to the spectrometer. Mathematical treatment of the spectrophotometric titrations was performed with factor analysis[130] and with the SPECFIT program.[131] Absorption spectra in solution were recorded using a Cary 5000 Varian spectrometer (quartz cell path length 1 mm, 200–800 nm domain). Absorption spectra in the solid state were recorded on a Lambda 900 PerkinElmer spectrometer equipped with an integration sphere (background recorded on MgO). Emission spectra were recorded upon excitation at 400 nm from powder samples at various temperatures from 3 K to 295 K with a Fluorolog 3-22 (Horiba Jobin–Yvon), equipped with a peltier-cooled photo multiplier tube (Hamamatsu R2658P), and corrected for the spectral response of the system. Excitation at 355 nm was obtained with the third harmonic of a pulsed Nd:YAG laser (Quantel Brilliant). The emitted light was collected with a telescope and focused onto a light-guide with a fibre bundle connected to a monochromator (Spex 270 M). Full spectra were recorded with a CCD (Spex Spectrum One), decay curves with a photomultiplier (Hamamatsu R928) and a digital oscilloscope (Tektronix TDS540B) or a multichannel scaler (Stanford Research SR430). For the latter the spectral bandwidth of the monochromator was set to 20 nm, thus giving the decay of the integral signal. Low temperatures were achieved with a closed cycle cryosystem (Janis, SHI-950) with the sample sitting in exchange gas for efficient cooling. Microcrystalline samples were mounted on copper plates with rubber cement. The copper plates were attached to the sample holder. Magnetization was measured using a Quantum Design VSM system (Department of Quantum Matter Physics, University of Geneva) in the range of 2–300 K. Solid samples of Cr_2Cl_6(tppz) (15.8 mg), Cr_2Cl_6(bbt) (16.0 mg), Cr_2Cl_6(ebbt) (4.7 mg), $[Cr_2(tpy)_2(bbt)](PF_6)_6$ (8.1 mg) and $[Cr_2(tpy)_2(ebbt)](PF_6)_6$ (14.9 mg) were immobilized in capsules, which were locked in a straw. The samples were introduced in the SQUID under an inert atmosphere of helium.

X-Ray crystallography

A summary of crystal data, intensity measurements and structure refinements for compounds (**1**) to (**15**) is collected in Tables S2, S3, S12, S17, S21, S26, S31 and S38 (ESI†). The crystals were mounted on MiTeGen raptor cryoloops with protection oil. X-ray data collections were performed with an Agilent SuperNova Dual diffractometer equipped with a CCD Atlas detector (Cu[Kα] radiation). The structures were solved by using direct methods.[140] Full-matrix least-square refinements on F^2 were performed with SHELX97.[141]

Specific refinement details. $[Cr(ebzpy)_2](CF_3SO_3)_3{\cdot}2CH_3CN$ (**4**): One triflate (of the 3 which are required for electroneutrality) and 0.5 CH_3CN molecules were extremely disordered. Because of the lack of well-defined features in the electron density map, several attempts to model this disorder didn't give satisfactory refinement. We thus performed SQUEEZE after exclusion of these disordered molecules (using Platon)[142] and found 8 voids of 123 $Å^3$ containing 75 electrons (corresponding to one CF_3SO_3) and 4 voids of 71 $Å^3$ containing 20 electrons (leading to 0.5 CH_3CN per formula unit).

$[Cr_2Cl_6(tppz)]{\cdot}3C_5H_9NO$ (**11**): The crystal was twinned. The twinned operation was a two-fold rotation along the *c* axis producing apparent Laue symmetry 6/*m*. The twin law [−1 0 0; 0 −1 0; 0 0 1] was applied in SHELXL,[141] including racemic twinning (four components). The twin fraction was 0.405(5) and the corresponding racemic twinning fractions were close to zero. Reflections *hk*2*l* were weak. There was almost translational symmetry with vector *c*/2. Indeed, the structure could be solved and refined in the smaller unit-cell with one complex and three solvent molecules, one of them disordered over two positions. The packing of this molecule produced the superstructure.

$[Cr_2Cl_6(bbt)]$ (**12**): A very large hole (around 1700 $Å^3$) was present in the structure. The squeeze/bypass procedure as implemented in Platon[142] was used to take care of the disordered solvent present in this hole (which could not be modelled otherwise). Around 505 electrons were found in each hole, which corresponded to about 4 acetone molecules per formula unit ($Z = 4$). These molecules were not added to the formula so that the density and absorption coefficients were somehow underestimated. *R* factors before squeezing: R_1 0.0788 and wR_2 0.22756 (all data).

CCDC 1542315–1542329† contain the supplementary crystallographic data.

Acknowledgements

Financial support from the Swiss National Science Foundation is gratefully acknowledged.

References

1 M. P. McDaniel, *Adv. Catal.*, 1985, **33**, 47–98.
2 S. E. Schaus, J. Brånalt and E. N. Jacobsen, *J. Org. Chem.*, 1998, **63**, 403–405.
3 A. G. Dossetter, T. F. Jamison and E. N. Jacobsen, *Angew. Chem., Int. Ed.*, 1999, **38**, 2398–2400.
4 A. M. McDaniel, H.-W. Tseng, N. H. Damrauer and M. P. Shores, *Inorg. Chem.*, 2010, **49**, 7981–7991.

5 A. M. McDaniels, H.-W. Tseng, E. A. Hill, N. H. Damrauer, A. K. Rappé and M. P. Shores, *Inorg. Chem.*, 2013, **52**, 1368–1378.
6 T. Mallah, S. Thiébaut, M. Verdaguer and P. Veillet, *Science*, 1993, **262**, 1554–1557.
7 V. Gadet, T. Mallah, I. Castro, M. Verdaguer and P. Veillet, *J. Am. Chem. Soc.*, 1992, **114**, 9213–9214.
8 R. L. Carlin and R. Burriel, *Phys. Rev. B: Condens. Matter*, 1983, **27**, 3012–3017.
9 M. Verdaguer, A. Bleuzen, V. Marvaud, J. Vaissermann, M. Seuleiman, C. Desplanches, A. Scuiller, C. Train, R. Garde, G. Gelly, C. Lomenech, I. Rosenman, P. Veillet, C. Cartier and F. Villain, *Coord. Chem. Rev.*, 1999, **190–192**, 1023–1047.
10 O. Kahn and B. Briat, *J. Chem. Soc., Faraday Trans. 2*, 1976, **72**, 268–281.
11 W. Liu, J. H. Christian, R. Al-Oweini, B. S. Bassil, J. van Tol, M. Atanasov, F. Neese, N. S. Dalal and U. Kortz, *Inorg. Chem.*, 2014, **53**, 9274–9283.
12 N. Novosel, D. Žilić, D. Pajić, M. Jurić, B. Perić, K. Zadro, B. Rakvin and P. Planinić, *Solid State Sci.*, 2008, **10**, 1387–1394.
13 L. S. Forster, *Chem. Rev.*, 1990, **90**, 331–353.
14 M. A. Jamieson, N. Serpone and M. Z. Hoffman, *Coord. Chem. Rev.*, 1981, **39**, 121–179.
15 A. D. Kirk, *Coord. Chem. Rev.*, 1981, **39**, 225–263.
16 T. H. Maiman, *Nature*, 1960, **187**, 493–494.
17 F.-F. Chen, Z.-Q. Chen, Z.-Q. Bian and C.-H. Huang, *Coord. Chem. Rev.*, 2010, **254**, 991–1010.
18 L. Aboshyan-Sorgho, M. Cantuel, S. Petoud, A. Hauser and C. Piguet, *Coord. Chem. Rev.*, 2012, **256**, 1644–1663.
19 T. J. Meyer, *Pure Appl. Chem.*, 1986, **58**, 1193–1206.
20 V. Balzani, A. Juris, M. Venturi, S. Campagna and S. Serroni, *Chem. Rev.*, 1996, **96**, 759–833.
21 V. Balzani, G. Bergamini, F. Marchioni and P. Ceroni, *Coord. Chem. Rev.*, 2006, **250**, 1254–1266.
22 F. R. Keene, *Dalton Trans.*, 2011, **40**, 2405–2418.
23 A. K. Pal and G. S. Hanan, *Chem. Soc. Rev.*, 2014, **43**, 6184–6197.
24 A. Winter and U. S. Schubert, *Chem. Soc. Rev.*, 2016, **45**, 5311–5357.
25 L. Helm and A. E. Merbach, *Chem. Rev.*, 2005, **105**, 1923–1960.
26 R. G. Pearson, R. A. Munson and F. Basolo, *J. Am. Chem. Soc.*, 1958, **80**, 504.
27 C.-A. Palma, M. Cecchini and P. Samori, *Chem. Soc. Rev.*, 2012, **41**, 3713–3730.
28 M. Murrie, S. Parsons, R. E. P. Winpenny, I. M. Atkinson and C. Benelli, *Chem. Commun.*, 1999, 285–286.
29 E. J. L. McInnes, S. Piligkos, G. A. Timco and R. E. P. Winpenny, *Coord. Chem. Rev.*, 2005, **249**, 2577–2590.
30 G. A. Timco, E. J. L. McInnes and R. E. P. Winpenny, *Chem. Soc. Rev.*, 2013, **42**, 1796–1806.
31 J. Springborg, *Adv. Inorg. Chem.*, 1988, **32**, 55–169.
32 G. Marinescu, M. Andruh, F. Lloret and M. Julve, *Coord. Chem. Rev.*, 2011, **255**, 161–185.
33 S. Decurtins, M. Gross, H. W. Schmalle and S. Ferlay, *Inorg. Chem.*, 1998, **37**, 2443–2448.
34 R. Sieber, S. Decurtins, H. Stoeckli-Evans, C. Wilson, D. Yufit, J. A. K. Howard, S. C. Capelli and A. Hauser, *Chem. – Eur. J.*, 2000, **6**, 361–368.
35 M. E. von Arx, E. Burattini, A. Hauser, L. van Pietserson, R. Pellaux and S. Decurtins, *J. Phys. Chem. A*, 2000, **104**, 883–893.
36 M. A. Subhan, T. Suzuki and S. Kaizaki, *J. Chem. Soc., Dalton Trans.*, 2001, 492–497.
37 H.-Z. Kou, B. C. Zhou, S. Gao and R.-J. Wang, *Angew. Chem., Int. Ed.*, 2003, **42**, 3288–3291.
38 Y. Li, Z. Jiang, M. Wang, J. Yuan, D. Liu, X. Yang, M. Chen, J. Yan, X. Li and P. Wang, *J. Am. Chem. Soc.*, 2016, **138**, 10041–10046.
39 D. Liu, Z. Jiang, M. Wang, X. Yang, H. Liu, M. Chen, C. N. Moorefield, G. R. Newkome, X. Li and P. Wang, *Chem. Commun.*, 2016, **52**, 9773–9776.
40 H. Iranmanesh, K. S. A. Arachchige, M. Bhadhade, W. A. Donald, J. Y. Liew, K. T.-C. Liu, E. T. Luis, E. G. Moore, J. R. Price, H. G. Yan, J.-X. Yang and J. E. Beves, *Inorg. Chem.*, 2016, **55**, 12737–12751.
41 B. Doistau, A. Tron, S. A. Denisov, G. Jonusauskas, N. D. McClenaghan, G. Gontard, V. Marvaud, B. Hasenknopf and G. Vives, *Chem. – Eur. J.*, 2014, **20**, 15799–15807.
42 B. Doistau, J.-L. Cantin, L.-M. Chamoreau, V. Marvaud, B. Hasenknopf and G. Vives, *Chem. Commun.*, 2015, **51**, 12916–12919.
43 R. Chakrabarty, P. S. Mukherjee and P. J. Stang, *Chem. Rev.*, 2011, **111**, 6810–6918.
44 M. Wang, K. Wang, C. Wang, M. Huang, X.-Q. Hao, M.-Z. Shen, G.-Q. Shi, Z. Zhang, B. Song, A. Cisneros, M.-P. Song, B. Xu and X. Li, *J. Am. Chem. Soc.*, 2016, **138**, 9258–9268.
45 E. C. Constable and A. M. W. Cargill-Thompson, *J. Chem. Soc., Dalton Trans.*, 1995, 1615–1627.
46 E. C. Constable, C. E. Housecroft, M. Neuburger, J. Schönle and J. A. Zampese, *Dalton Trans.*, 2014, **43**, 7227–7235.
47 M. Maestri, F. Bolletta, N. Serpone, L. Moggi and V. Balzani, *Inorg. Chem.*, 1976, **15**, 2048–2051.
48 M. Cantuel, G. Bernardinelli, D. Imbert, J.-C. G. Bunzli, G. Hopfgartner and C. Piguet, *J. Chem. Soc., Dalton Trans.*, 2002, 1929–1940.
49 M. Cantuel, F. Gumy, J.-C. G. Bunzli and C. Piguet, *Dalton Trans.*, 2006, 2647–2660.
50 L. Aboshyan-Sorgho, C. Besnard, P. Pattison, K. R. Kittilstved, A. Aebischer, J.-C. G. Bünzli, A. Hauser and C. Piguet, *Angew. Chem., Int. Ed.*, 2011, **50**, 4108–4112.
51 Y. Suffren, D. Zare, S. V. Eliseeva, L. Guénée, H. Nozary, T. Lathion, L. Aboshyan-Sorgho, S. Petoud, A. Hauser and C. Piguet, *J. Phys. Chem. C*, 2013, **117**, 26957–26963.

52 D. Zare, Y. Suffren, L. Guénée, S. V. Eliseeva, H. Nozary, L. Aboshyan-Sorgho, S. Petoud, A. Hauser and C. Piguet, *Dalton Trans.*, 2015, **44**, 2529–2540.
53 Y. Suffren, B. Golesorkhi, D. Zare, L. Guénée, H. Nozary, S. V. Eliseeva, S. Petoud, A. Hauser and C. Piguet, *Inorg. Chem.*, 2016, **55**, 9964–9972.
54 I. Bertini, P. Turano and A. J. Vila, *Chem. Rev.*, 1993, **93**, 2833–2932.
55 E. Rousset, D. Chartrand, I. Ciofini, V. Marvaud and G. S. Hanan, *Chem. Commun.*, 2015, **51**, 9261–9264.
56 V. Balzani, A. Credi and M. Venturi, *ChemSusChem*, 2008, **1**, 26–58.
57 M. Schulze, V. Kunz, P. D. Frischmann and F. Würthner, *Nat. Chem.*, 2016, **8**, 576–583.
58 J. P. Collin, S. Guillerez, J. P. Sauvage, F. Barigelletti, L. De Cola, L. Flamigni and V. Balzani, *Inorg. Chem.*, 1991, **30**, 4230–4238.
59 C. K. Jorgensen, *Adv. Chem. Phys.*, 1963, **5**, 33–146.
60 A. B. P. Lever, *Inorganic Electronic Spectroscopy*, Elsevier, Amsterdam, Oxford, New York, Tokyo, 2nd edn, 1984, p. 126.
61 S. K. Padhi, D. Saha, R. Sahu, J. Subramanian and V. Manivannan, *Polyhedron*, 2008, **27**, 1714–1720.
62 T. J. Morsing, S. P. A. Sauer, H. Weihe, J. Bendix and A. Døssing, *Inorg. Chim. Acta*, 2013, **396**, 72–77.
63 C. Creutz and H. Taube, *J. Am. Chem. Soc.*, 1969, **91**, 3988–3989.
64 R. A. Marcus, *J. Chem. Phys.*, 1956, **24**, 966–978.
65 R. A. Marcus, *Rev. Mod. Phys.*, 1993, **65**, 599–610.
66 A. Heckmann and C. Lambert, *Angew. Chem., Int. Ed.*, 2012, **51**, 326–392.
67 M. B. Robin and P. Day, in *Advances in Inorganic Chemistry and Radiochemistry*, ed. H. J. Emeléus and A. G. Sharpe, Academic Press, 1968, vol. 10, pp. 247–422.
68 P. Day, N. S. Hush and R. J. H. Clarck, *Philos. Trans. R. Soc., A*, 2008, **366**, 5–14.
69 J. P. Sauvage, J. P. Collin, J. C. Chambron, S. Guillerez, C. Coudret, V. Balzani, F. Barigelletti, L. De Cola and L. Flamigni, *Chem. Rev.*, 1994, **94**, 993–1019.
70 H. Ozawa, M. Baghernejad, O. A. Al-Owaedi, V. Kaliginedi, T. Nagashima, J. Ferrer, T. Wandlowski, V. M. García-Suárez, P. Broekmann, C. J. Lambert and M.-A. Haga, *Chem. – Eur. J.*, 2016, **22**, 12732–12740.
71 J.-P. Collin, P. Laine, J.-P. Launay, J.-P. Sauvage and A. Sour, *J. Chem. Soc., Chem. Commun.*, 1993, 434–435.
72 H. Torieda, K. Nozaki, A. Yoshimura and T. Ohno, *J. Phys. Chem. A*, 2004, **108**, 4819–4829.
73 H. Torieda, A. Yoshimura, K. Nozaki, S. Sakai and T. Ohno, *J. Phys. Chem. A*, 2002, **106**, 11034–11044.
74 B. Schlicke, P. Belser, L. De Cola, E. Sabbioni and V. Balzani, *J. Am. Chem. Soc.*, 1999, **121**, 4207–4214.
75 F. Barigelletti, L. Flamigni, V. Balzani, J.-P. Collin, J.-P. Sauvage, A. Sour, E. C. Constable and A. M. W. Cargill-Thompson, *J. Am. Chem. Soc.*, 1994, **116**, 7692–7699.
76 M. Bar, D. Maity, S. Das and S. Baitalik, *Dalton Trans.*, 2016, **45**, 17241–17253.
77 D. L. Dexter, *J. Chem. Phys.*, 1953, **21**, 836–850.
78 S. S. Skourtis, C. Liu, P. Antoniou, A. M. Virshup and D. N. Beratan, *Proc. Natl. Acad. Sci. U. S. A.*, 2016, **113**, 8115–8120.
79 C. C. Scarborough, S. Sproules, T. Weyhermueller, S. DeBeer and K. Wieghardt, *Inorg. Chem.*, 2011, **50**, 12446–12462.
80 C. C. Scarborough, K. M. Lancaster, S. DeBeer, T. Weyhermüller, S. Sproules and K. Wieghardt, *Inorg. Chem.*, 2012, **51**, 3718–3732.
81 K. D. Barker, K. A. Barnett, S. M. Connell, J. W. Glaeser, A. J. Wallace, J. Wildsmith, B. J. Herbert, J. F. Wheeler and N. A. P. Kane-Maguire, *Inorg. Chim. Acta*, 2001, **316**, 41–49.
82 M. Isaacs, A. G. Sykes and S. Ronco, *Inorg. Chim. Acta*, 2006, **359**, 3847–3854.
83 J. Schönle, E. C. Constable, C. E. Housecroft and M. Neuburger, *Inorg. Chem. Commun.*, 2015, **53**, 80–83.
84 J. Schönle, E. C. Constable, C. E. Housecroft, A. Prescimone and J. A. Zampese, *Polyhedron*, 2015, **89**, 182–188.
85 L. Pazderski, T. Pawlak, J. Sitkowski, L. Kozerski and E. Szlyk, *Magn. Reson. Chem.*, 2011, **49**, 237–241.
86 E. C. Constable, *Adv. Inorg. Chem. Radiochem.*, 1986, **30**, 69–121.
87 M. L. Scudder, H. A. Goodwin and I. G. Dance, *New J. Chem.*, 1999, **23**, 695–705.
88 S. Grimme, *Angew. Chem., Int. Ed.*, 2008, **47**, 3430–3434.
89 R. Zhao and R.-Q. Zhang, *Phys. Chem. Chem. Phys.*, 2016, **18**, 15452–25457.
90 C. Piguet, J.-C. G. Bünzli, G. Bernardinelli and A. F. Williams, *Inorg. Chem.*, 1993, **32**, 4139–4149.
91 W. A. Wickramasinghe, P. H. Bird, M. A. Jamieson and N. Serpone, *J. Chem. Soc., Chem. Commun.*, 1979, **1979**, 798–800.
92 W. A. Wickramasinghe, P. H. Bird and N. Serpone, *Inorg. Chem.*, 1982, **21**, 2694–2698.
93 N. Cloete, H. G. Visser and A. Roodt, *Acta Crystallogr., Sect. E: Struct. Rep. Online*, 2007, **63**, m45–m47.
94 W. Zhang, W.-H. Sun, S. Zhang, J. Hou, K. Wedeking, S. Schultz, R. Fröhlich and H. Song, *Organometallics*, 2006, **25**, 1961–1969.
95 R. S. Bitzer, C. A. L. Filgueiras, J. G. S. Lopes, P. S. Santos and M. H. Herbst, *Transition Met. Chem.*, 2005, **30**, 636–642.
96 R. C. Rocha, F. N. Rein, H. Jude, A. P. Shreve, J. J. Concepcion and T. J. Meyer, *Angew. Chem., Int. Ed.*, 2008, **47**, 503–506.
97 B. A. Albani, B. Pena, S. Saha, J. K. White, A. M. Schaeffer, K. R. Dunbar and C. Turro, *Chem. Commun.*, 2015, **51**, 16522–16525.
98 R. Davidson, J.-H. Liang, D. Costa Milan, B.-W. Mao, R. J. Nichols, S. J. Higgins, D. S. Yufit, A. Beeby and P. J. Low, *Inorg. Chem.*, 2015, **54**, 5487–5494.
99 M. Graf, H. Stoeckli-Evans, A. Escuer and R. Vicente, *Inorg. Chim. Acta*, 1997, **257**, 89–97.
100 T. Nagashima, T. Nakabayashi, T. Suzuki, K. Kanaizuka, H. Ozawa, Y.-W. Zhong, S. Masaoka, K. Sakai and M.-A. Haga, *Organometallics*, 2014, **33**, 4893–4904.

101 C.-J. Yao, Y.-W. Zhong and J. Yao, *Inorg. Chem.*, 2013, **52**, 4040–4045.
102 N. Yoshikawa, S. Yamabe, N. Kanehisa, T. Inoue, H. Takashima and K. Tsukahara, *J. Phys. Org. Chem.*, 2011, **24**, 1110–1118.
103 Á. J. Pérez-Jiménez, J. C. Sancho-García and J. M. Pérez-Jordá, *J. Chem. Phys.*, 2005, **123**, 134309.
104 M. P. Johansson and J. Olsen, *J. Chem. Theor. Comput.*, 2008, **4**, 1460–1471.
105 W. Ouellette, B.-K. Koo, E. Burkholder, V. Golub, C. J. O'Connor and J. Zubieta, *Dalton Trans.*, 2004, 1527–1538.
106 S. Jones, J. M. Vargas, S. Pellizzeri, C. J. O'Connor and J. Zubieta, *Inorg. Chim. Acta*, 2013, **395**, 44–57.
107 S. Dev, S. Maheshwari and A. R. Choudhury, *RSC Adv.*, 2015, **5**, 26932–26940.
108 E. Kryachko and S. Scheiner, *J. Phys. Chem. A*, 2004, **108**, 2527–2535.
109 V. Grosshenny, F. M. Romero and R. Ziessel, *J. Org. Chem.*, 1997, **62**, 1491–1500.
110 G. A. Bain and J. F. Berry, *J. Chem. Educ.*, 2008, **85**, 532–536.
111 J.-P. Launay and M. Verdaguer, *Electrons in Molecules from Basic Principles to Molecular Electronics*, Oxford University Press, Oxford, 2014.
112 O. Kahn, *Molecular Magnetism*, VCH Publishers, Weinheim, 1993, pp. 150–164.
113 Q. Ren and Z. Chen, *J. Mol. Struct. (THEOCHEM)*, 2005, **719**, 159–168.
114 M. Atanasov, P. Comba and C. A. Daul, *Inorg. Chem.*, 2008, **47**, 2449–2463.
115 H. Witzke, *Theor. Chim. Acta*, 1971, **20**, 171–185.
116 D. L. Wood, J. Ferguson, K. Knox and J. F. Dillon, *J. Chem. Phys.*, 1963, **39**, 890–898.
117 J. Ferguson, *Prog. Inorg. Chem.*, 1970, **12**, 159–293.
118 C. K. Jorgensen, *Modern Aspects of Ligand Field Theory*, North Holland Publishing Company, Amsterdam, 1971, ch. 23 and 26.
119 A. Hauser, M. Maeder, W. T. Robinson, R. Murugesan and J. Ferguson, *Inorg. Chem.*, 1987, **26**, 1331–1338.
120 S. Otto, M. Grabolle, C. Förster, C. Kreitner, U. Resch-Genger and K. Heinze, *Angew. Chem., Int. Ed.*, 2015, **54**, 11572–11576.
121 A. Harriman, A. Khatyr, R. Ziessel and A. C. Benniston, *Angew. Chem., Int. Ed.*, 2000, **39**, 4287–4290.
122 A. C. Benniston, G. Chapman, A. Harriman, M. Mehrabi and C. A. Sams, *Inorg. Chem.*, 2004, **43**, 4227–4233.
123 T. V. Duncan, K. Song, S.-T. Hung, I. Miloradovic, A. Nayak, A. Persoons, T. Verbiest, M. J. Therien and K. Clays, *Angew. Chem., Int. Ed.*, 2008, **47**, 2978–2981.
124 F. Castelli and L. S. Forster, *J. Am. Chem. Soc.*, 1975, **97**, 6306–6309.
125 M. E. Starzak, in *Mathematical Methods in Chemistry and Physics*, Plenum Press, New York, 1989, pp. 289–357.
126 B. Henderson and G. F. Imbusch, *Optical Spectroscopy of Inorganic Solids*, Clarendon Press, Oxford, 1989.
127 Y. Shen, T. Riedener and K. L. Bray, *Phys. Rev. B: Condens. Matter*, 2000, **61**, 11460–11471.
128 A. Zaïm, S. V. Eliseeva, L. Guénée, H. Nozary, S. Petoud and C. Piguet, *Chem. – Eur. J.*, 2014, **20**, 12172–12182.
129 J. Yuasa and S. Fukuzumi, *J. Am. Chem. Soc.*, 2008, **130**, 566–575.
130 (*a*) E. R. Malinowski and D. G. Howery, *Factor Analysis in Chemistry*, Wiley, New York, Chichester, 1980; (*b*) H. Gampp, M. Maeder, C. J. Meyer and A. Zuberbühler, *Talanta*, 1986, **33**, 943–951; (*c*) B. R. Hall, L. E. Manck, I. S. Tidmarsh, A. Stephenson, B. F. Taylor, E. J. Blaikie, D. A. Vander Griend and M. D. Ward, *Dalton Trans.*, 2011, **40**, 12132–12145.
131 (*a*) H. Gampp, M. Maeder, C. J. Meyer and A. Zuberbühler, *Talanta*, 1985, **32**, 1133–1139; (*b*) M. Maeder and P. King, Analysis of Chemical Processes, Determination of the Reaction Mechanism and Fitting of Equilibrium and Rate Constants, in *Chemometrics in Practical Applications*, ed. K. Varmuza, InTech, 2012, ISBN: 978-953-51-0438-4, DOI: 10.5772/31896; (*c*) Specfit/32 from ReactLab Equilibria: http://jplusconsulting.com/products/reactlab-equilibria/.
132 A. Duerrbeck, S. Gorelik, J. Hobley, J. Wu, A. Hor and N. Long, *Chem. Commun.*, 2015, **51**, 8656–8659.
133 C. Piguet, *Chem. Commun.*, 2010, **46**, 6209–6231.
134 G. Ercolani, C. Piguet, M. Borkovec and J. Hamacek, *J. Phys. Chem. B*, 2007, **111**, 12195–12203.
135 A. Escande, L. Guénée, K.-L. Buchwalder and C. Piguet, *Inorg. Chem.*, 2009, **48**, 1132–1147.
136 A. Albert and J. N. Phillips, *J. Chem. Soc.*, 1956, 1294–1304.
137 A. W.-H. Mau, J. H. Overbeek, J. W. Loder and W. H. F. Sasse, *J. Chem. Soc., Faraday Trans. 2*, 1986, **82**, 869–876.
138 V. Grosshenny and R. Ziessel, *J. Organomet. Chem.*, 1993, **453**, C19–C22.
139 (*a*) E. C. Constable and M. D. Ward, *J. Chem. Soc., Dalton Trans.*, 1990, 1405–1409; (*b*) E. C. Constable and A. M. W. C. Thompson, *J. Chem. Soc., Dalton Trans.*, 1992, 3467–3475.
140 (*a*) SHELXS97 G. M. Sheldrick, *Acta Crystallogr., Sect. A: Fundam. Crystallogr.*, 2008, **64**, 112–122; (*b*) SIR97 A. Altomare, M. C. Burla, M. Camalli, G. L. Cascarano, C. Giacovazzo, A. Guagliardi, A. G. Moliterni, G. Polidori and R. Spagna, *J. Appl. Crystallogr.*, 1999, **32**, 115–119; (*c*) SIR92: A. Altomare, G. Cascarano, C. Giacovazzo and A. Guagliardi, *J. Appl. Crystallogr.*, 1993, **26**, 343–350.
141 G. M. Sheldrick, *Acta Crystallogr., Sect. C: Struct. Chem.*, 2015, **71**, 3–8.
142 P. van der Sluis and A. L. Spek, *Acta Crystallogr., Sect. A: Fundam. Crystallogr.*, 1990, **46**, 194–201.